

Crystal Packing Modulation of the Strength of Resonance-Assisted Hydrogen Bonds and the Role of Resonance-Assisted Pseudoring Stacking in Geminal Amido Esters: Study Based on Crystallography and Theoretical Calculations

Perumal Venkatesan, Subbiah Thamotharan,* M. Judith Percino, and Andivelu Ilangovan*



Cite This: *Cryst. Growth Des.* 2021, 21, 779–798



Read Online

ACCESS |



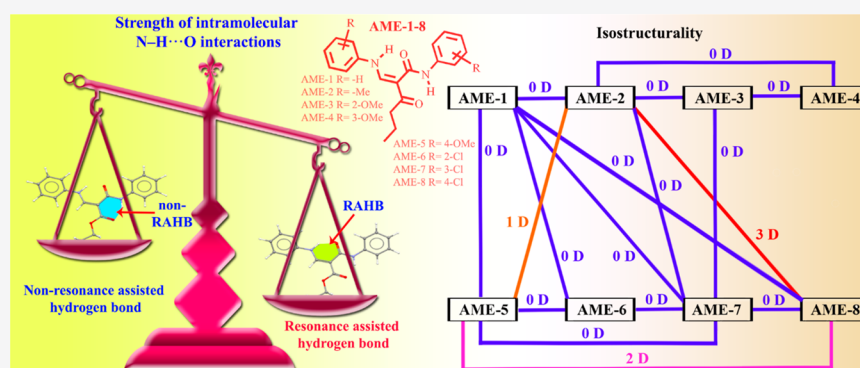
Metrics & More



Article Recommendations



Supporting Information



ABSTRACT: A detailed experimental and theoretical investigation of a series of substituted geminal amido esters (ethyl (*E*)-3-(arylamino)-2-(arylcabamoyl)prop-2-enoate, **AME-1–8**) leading to the identification of a unique angularly fused pseudotriangular (*S*(6),*S*(6),*S*(6)) ring system stabilized by an intramolecular resonance-assisted hydrogen bond (RAHB) and a non-RAHB are presented in addition to weak intermolecular interactions. An analysis of X-ray and theoretical models reveals that the strength of the intramolecular RAHB (N1–H1_N...O1) varies in a wide range (6.9–11.4 kcal mol⁻¹) due to crystal-packing constraints arising from different aromatic ring substitutions. However, the effect is less significant and the strength differs only in a narrow range (8.2–9.9 kcal mol⁻¹) in the case of non-RAHB. The downfield shift ($\delta \sim 12.3$) observed for the N–H_{aniline} signal in ¹H NMR spectra of **AME-1–8** is due to the presence of intramolecular RAHB. A PIXEL energy analysis suggests that the molecular dimer formed by stacking of RAHB pseudorings is found to be strong ($E_{\text{tot}} = -14.4$ to -17.9 kcal mol⁻¹), and this dimer forms the basic motif in most of the structures reported herein. A detailed analysis of the isostructurality suggests that the basic motif exists in most of the structural combinations. The weak intermolecular C–H...O, C–H...Cl, and C–H... π interactions play a vital role in the stabilization of these crystal structures, as evaluated by PIXEL and Bader’s quantum theory of atoms in molecules approach (QTAIM). A lattice energy analysis suggests that the Coulombic contribution and total lattice energies are higher in the *para*-substituted compounds (**AME-2**, **AME-5**, and **AME-8**) in comparison to the other isomeric compounds. Further, the crystal packing of these compounds is analyzed on the basis of the energy frameworks. It shows that most of the crystals show similar 3D topologies, suggesting that these compounds may have similar mechanical behavior.

INTRODUCTION

Instituting novel hydrogen-bonding networks is central to supramolecular design in organic, coordination, and organometallic compounds. Since the introduction of “The Hydrogen Bond” in 1920 by Latimer and Rodebush, 100 years have passed and its imperative role in many areas of chemistry continues.¹ During the past few decades, different types of hydrogen bonds (HBs), i.e. (i) charge-assisted hydrogen bonds (CAHBs),^{2–4} low-barrier hydrogen bonds (LBHBs),^{5,6} dihydrogen bonds (DHBs),^{7,8} and resonance-assisted hydrogen bonds (RAHBs)^{9,10} have been identified and investigated.¹¹

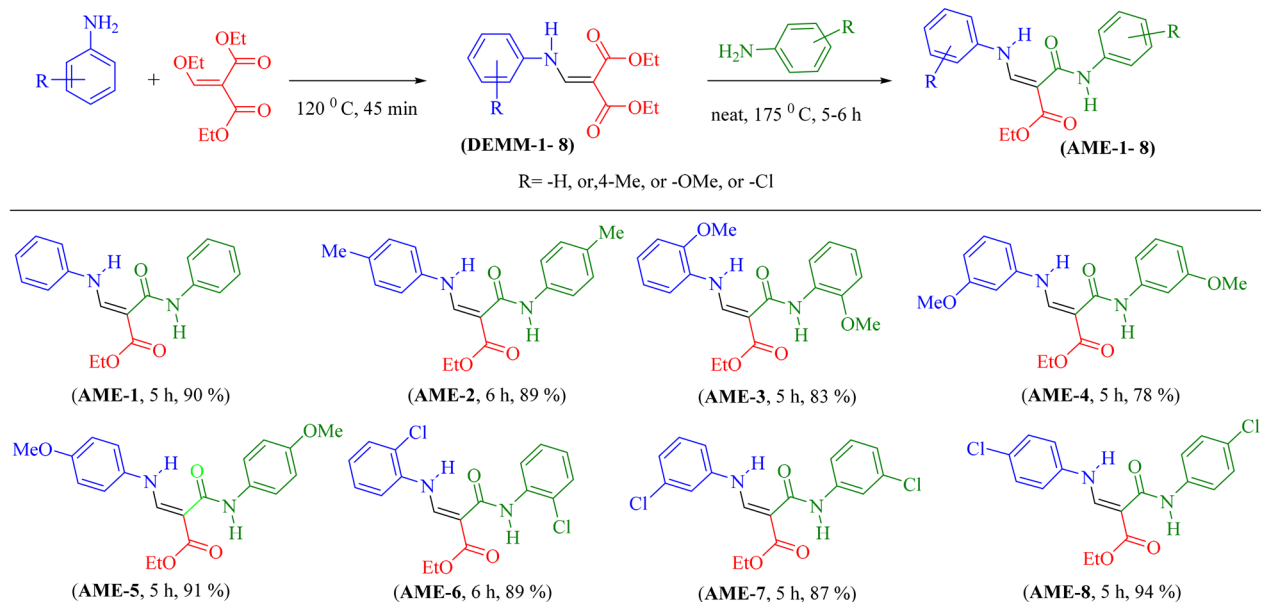
Among them, the RAHB is the most frequent concept used in structural chemistry.^{6,9–14} It was first proposed by Gilli et al.^{9,10} in the late 1980s. The RAHB is stronger and significantly shorter than the conventional hydrogen bond (HB), observed

Received: July 21, 2020

Revised: December 13, 2020

Published: December 29, 2020



Scheme 1. Synthesis of Ethyl (2*E*)-3-(Arylamino)-2-(arylcabamoyl)acrylate (AME-1–8)

among neutral molecules showing O–H···O/N–H···O interactions conjugated with multiple π -bonds. The unusual stabilization energy for the RAHB is attributed to partial delocalization of the π -electrons along with their respective HB systems.⁷ This simple and powerful concept of RAHB finds significant use in synthetic transformations, the design of chelating pockets for coordination, molecular recognition, the design of molecular switches, and crystal engineering, among many other applications in organic chemistry.¹ Further, the (*R*)-binol-based chiral aldehydes which form RAH-bonded imines with amino acids have been developed and used as shift reagents.¹⁵ In addition, the same (*R*)-binol-based compounds have been used in the deracemization of amino acids whereby RAHBs activate epimerization of the imine intermediates.^{16,17} Compounds (*S*-(benzothiazol-2-yl)-4-hydroxyisophthalaldehyde¹⁸ and *N*-(2-pyridyl)-2-oxo-1-naphthylidene methyl amine)¹⁹ showing RAHBs have been used as chemosensors and colorimetric agents for the detection of cyanides, even in aqueous media.^{18,19} Also, the RAHB is used to improve the mesomorphic behavior of supramolecular liquid crystals formed from azopyridines with different linear alkyl chains²⁰ and control of the Diaza-Cope rearrangement^{21–23} and the configurational isomerization of push–pull thiazolidinone derivatives.²⁴

The intramolecular RAHB was successfully studied in a wide range of systems such as β -diketone enols,⁹ 1,3-diketone aryl hydrazones,²⁵ and α -enaminones.²⁶ Similarly, an intermolecular RAHB was examined in β -diketone enols,²⁵ *anti*- β -ketoarylhydrazones, NH-pyrazoles,²⁷ secondary enaminones,²⁸ etc. Furthermore, both intra- and intermolecular RAHBs showing O–H···O, N–H···O, O–H···N, and O–H···S interactions have been investigated with the aid of experimental and theoretical methods.^{29–32} The resonance-induced charge transfer process observed in RAHBs decreases the vibrational frequencies and shifts ¹H NMR signals downfield.^{33,34} On the other hand, the effect of substitution on the strength of the RAHB existing in mono- and disubstituted *o*-hydroxybenzaldehyde derivatives was explored.³⁵ The authors also explained how different substituent

groups (π -electron-donating groups –NH₂, –OH, and –F; π -electron-withdrawing groups –NO₂, –NO, and CN) influence the stability of the RAHB in these compounds. Further, it has been concluded that electron-donating groups at *ortho/para* to the –OH group enhanced the formation of a RAHB. However, electron-withdrawing functionalities *ortho/para* to the –OH group decreased the formation of a RAHB.³⁵ Steric and electronic factors also interplay in strength of a RAHB in β -ketoarylhydrazones.^{36,37} The studies reported above clearly suggest the potential importance of RAHB-containing compounds. After Gilli's initial proposal that the formation as well as variation in the strength of a RAHB takes place due to π -polarization of a hydrogen-bonding C=O group,³⁸ different researchers proposed the origin of the RAHB. Fonseca Guerra et al.³⁹ suggested electrostatic and donor–acceptor orbital interactions as well as movement of the donor and acceptor groups closer in proximity due to π -resonance as the reason for an RAHB.^{1,39,40} Further, computational studies suggested that the effects of the RAHB originated from geometric constraints of the σ -framework.¹ Cole and her co-workers described the intramolecular charge transfer and the molecular hyperpolarizability of geminal amido esters with different donor– π -acceptor (D– π -A) moieties on the basis of DFT and X-ray/neutron diffraction studies.⁴¹ They also identified that the amido ester derivative with 4-NO₂ and 2,5-OMe substituents showed promising nonlinear optical characteristics. Further, the role of intermolecular interactions present in these structures was not explored in their studies.⁴¹

In the present study on geminal amido ester derivatives AME-1–8 (ethyl (2*E*)-3-(arylamino)-2-(arylcabamoyl)prop-2-enoate), we have now found that, in addition to the effect of the π -polarization of the C=O group, due to the conjugated aromatic ring and its substituent groups, the crystal packing also contributes to the modulation of the strength of RAHBs. An unusual angularly fused tricyclic pseudoring system has been found. The crystal packing effect was studied on the basis of X-ray and theoretical models with the aid of Bader's quantum theory of atoms in molecules (QTAIM) approach.^{42,43} A systematic analysis of noncovalent interactions

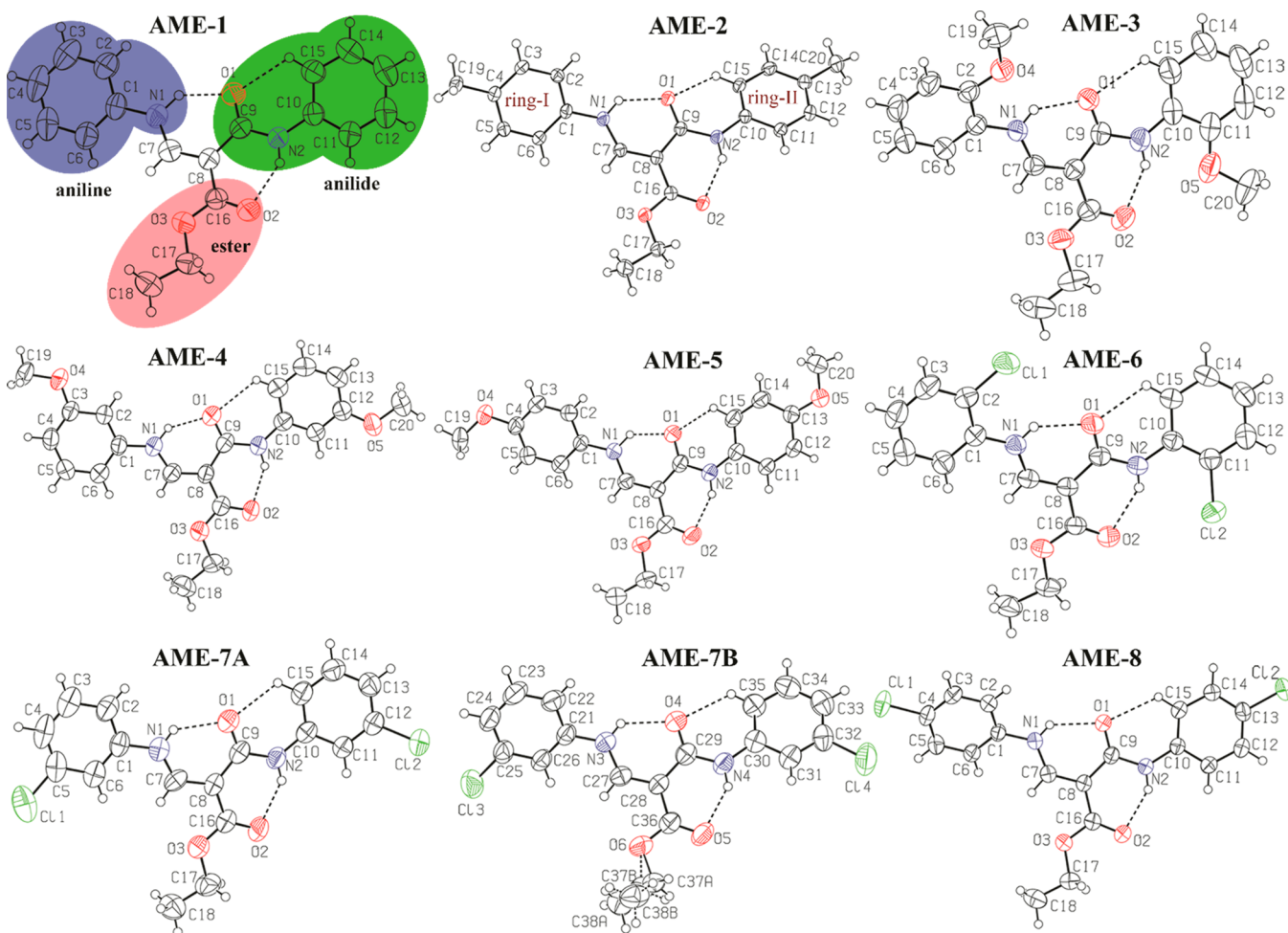


Figure 1. Thermal ellipsoid plots of AME-1–8 with the ellipsoids drawn at the 50% probability level. The atom-labeling scheme and invariant intramolecular N–H···O and C–H···O interactions are shown in dashed lines. The aniline, anilide, and ester moieties in AME-1 are shaded with three different colors.

with the aid of experimental, PIXEL, and QTAIM calculations was carried out to understand how the weak C–H···O and C–H··· π interactions and other weak interactions participate in the stabilization of the crystal structures of AME-1–8. A Hirshfeld surface (HS) analysis^{44–46} and 2D fingerprint (FP) analysis^{47,48} have been used to analyze the relative contributions of different intermolecular interactions existing in these crystal structures to understand the effect of different substituents.

EXPERIMENTAL SECTION

General Procedure for the Synthesis of Diethyl [(Arylamino)methylidene]propanedioate (DEMM-1–8). A mixture of the substituted aniline (4 mmol) and diethyl ethoxymethylenemalonate (4 mmol) was heated at 120 °C for 45 min under solvent-free conditions to give the corresponding diethyl [(arylamino)methylidene]propanedioates (DEMM-1–8, Scheme 1) in good yield (>98%). The products were characterized by spectral data, which are comparable with those in our earlier report.⁴⁹

General Procedure for the Synthesis of Ethyl (2E)-3-(Arylamino)-2-(arylcabamoyl)prop-2-enoate (AME-1–8). A mixture of diethyl [(arylamino)methylidene]propanedioate (DEMM-1–8, 4 mmol) and the respective aniline (4 mmol) was heated at 170 °C for 5–6 h under solvent-free conditions (Scheme 1). After completion of the reaction, the products were purified using column chromatography (silica gel, hexane/EtOAc, 8/2 v/v) to give the corresponding products in 80–95% yield. All of the purified

compounds were characterized by ¹H and ¹³C NMR and single-crystal X-ray diffraction studies. A detailed synthesis procedure for all of the individual compounds AME-1–8 and the spectral data are given in the Supporting Information.

Single-Crystal X-ray Diffraction. Single crystals of compounds AME-1–8 were grown by a slow evaporation method (at room temperature, 296 K) using a hexane/ethyl acetate solvent mixture (8/2, v/v). The X-ray intensity data collections were carried out at room temperature (296 K) on a Bruker SMART APEX II CCD diffractometer (APEX2, SAINT, and SADABS; Bruker AXS Inc., Madison, WI, USA) using Mo K α radiation ($\lambda = 0.71073$ Å). All of the structures except AME-8 were solved by direct methods using the program SHELXS-2014.⁵⁰ The isomorphous approach was employed for AME-8 using the coordinates of the AME-2 structure. All of the non-hydrogen atoms were refined by full-matrix least squares on F^2 using SHELXL-2018/3.⁵⁰ The positions of amine H were located from a difference Fourier map and refined freely along with their isotropic displacement parameters. All of the remaining H atoms were placed at calculated positions using a riding model approach. All of the structures in the present study are ordered except for AME-7. The ethyl group (atoms C36 and C37) of the ester moiety in AME-7 was disordered over two orientations, and the occupancy values for the major and minor component were refined to be 0.64(2) and 0.36(2), respectively. The ORTEP and crystal packing diagrams were generated using the programs PLATON⁵¹ and Mercury,^{52,53} respectively.

Gas-Phase Structural Optimization. All of the quantum chemical calculations were performed with the Gaussian16 program

Table 1. Crystal Data and Refinement Parameters for AME-1–8

| | AME-1 | AME-2 | AME-3 | AME-4 |
|---|---|---|---|---|
| CCDC no. | 665885 | 678846 | 655619 | 664991 |
| empirical formula | C ₁₈ H ₁₈ N ₂ O ₃ | C ₂₀ H ₂₂ N ₂ O ₃ | C ₂₀ H ₂₂ N ₂ O ₃ | C ₂₀ H ₂₂ N ₂ O ₃ |
| formula wt | 310.34 | 338.39 | 370.39 | 370.39 |
| cryst syst | monoclinic | monoclinic | monoclinic | monoclinic |
| space group | P2 ₁ /c | C2/c | P2 ₁ /n | P2 ₁ /c |
| a (Å) | 7.1382(14) | 18.795(4) | 9.0693(6) | 12.500(3) |
| b (Å) | 13.398(3) | 11.995(2) | 16.8073(11) | 19.953(4) |
| c (Å) | 17.100(3) | 15.567(3) | 13.1818(9) | 7.6459(15) |
| α (deg) | 90.0 | 90.0 | 90.0 | 90.0 |
| β (deg) | 94.55(3) | 91.66(2) | 105.118(10) | 97.90(3) |
| γ (deg) | 90.0 | 90.0 | 90.0 | 90.0 |
| V (Å ³) | 1630.3(6) | 3508.0(12) | 1939.8(2) | 1888.9(7) |
| Z | 4 | 8 | 4 | 4 |
| calcd density (Mg/m ³) | 1.264 | 1.281 | 1.268 | 1.302 |
| absorption (mm ⁻¹) | 0.087 | 0.087 | 0.092 | 0.094 |
| F(000) | 656 | 1440 | 784 | 784 |
| θ (deg) | 3.0–27.5 | 2.0–27.6 | 2.0–28.0 | 3.1–27.4 |
| limiting indices | | | | |
| h | −9 ≤ h ≤ 8 | −24 ≤ h ≤ 24 | −11 ≤ h ≤ 11 | −16 ≤ h ≤ 16 |
| k | −17 ≤ k ≤ 17 | −15 ≤ k ≤ 14 | −21 ≤ k ≤ 21 | −25 ≤ k ≤ 25 |
| l | −22 ≤ l ≤ 22 | −20 ≤ l ≤ 19 | −17 ≤ l ≤ 17 | −9 ≤ l ≤ 9 |
| no. of collected/unique rflns | 15589/3724 | 14356/4011 | 22003/4563 | 18346/4271 |
| no. of data/restraints/params | 3724/0/217 | 4011/0/237 | 4563/0/255 | 4271/0/255 |
| goodness of fit (GOF) on F ² | 1.04 | 1.06 | 1.05 | 1.01 |
| final R indices (I > 2σ(I)) | | | | |
| R1 | 0.041 | 0.045 | 0.045 | 0.059 |
| wR2 | 0.108 | 0.112 | 0.1250 | 0.117 |
| R indices (all data) | | | | |
| R1 | 0.069 | 0.065 | 0.057 | 0.13 |
| wR2 | 0.116 | 0.129 | 0.1340 | 0.139 |
| largest difference peak/hole (e Å ⁻³) | 0.220/−0.098 | 0.267/−0.256 | 0.173/−0.151 | 0.232/−0.130 |
| | AME-5 | AME-6 | AME-7 | AME-8 |
| empirical formula | C ₂₀ H ₂₂ N ₂ O ₃ | C ₁₈ H ₁₆ Cl ₂ N ₂ O ₃ | C ₁₈ H ₁₆ Cl ₂ N ₂ O ₃ | C ₁₈ H ₁₆ Cl ₂ N ₂ O ₃ |
| CCDC no. | 804832 | 665886 | 804833 | 804925 |
| formula wt | 370.39 | 379.23 | 379.23 | 379.23 |
| cryst syst | monoclinic | monoclinic | triclinic | monoclinic |
| space group | C2/c | P2 ₁ /n | P $\bar{1}$ | C2/c |
| a (Å) | 24.6940(6) | 14.947(3) | 7.4613(2) | 18.6444(4) |
| b (Å) | 12.4970(2) | 7.7889 (16) | 15.6554(4) | 12.0202(3) |
| c (Å) | 14.7603(5) | 15.366(3) | 15.6825(4) | 15.6673(4) |
| α (deg) | 90.0 | 90.0 | 84.442(2) | 90.0 |
| β (deg) | 125.668(2) | 91.76(3) | 87.6120(10) | 90.224(10) |
| γ (deg) | 90.0 | 90.0 | 77.6080(10) | 90.0 |
| V (Å ³) | 3700.56(18) | 1788.1(6) | 1780.37(8) | 3511.16(15) |
| Z | 8 | 4 | 4 | 8 |
| calcd density (Mg/m ³) | 1.33 | 1.41 | 1.42 | 1.44 |
| absorption (mm ⁻¹) | 0.096 | 0.382 | 0.384 | 0.390 |
| F(000) | 1568 | 784 | 784 | 1568 |
| θ (deg) | 1.9–25.0 | 3.2–27.5 | 1.3–25.2 | 2.0–31.0 |
| limiting indices | | | | |
| h | −29 ≤ h ≤ 29 | −19 ≤ h ≤ 19 | −8 ≤ h ≤ 8 | −26 ≤ h ≤ 26 |
| k | −14 ≤ k ≤ 14 | −10 ≤ k ≤ 10 | −17 ≤ k ≤ 17 | −17 ≤ k ≤ 16 |
| l | −17 ≤ l ≤ 17 | −19 ≤ l ≤ 18 | −17 ≤ l ≤ 17 | −22 ≤ l ≤ 16 |
| no. of collected/unique rflns | 30836/3237 | 16747/4045 | 25837/5013 | 20813/5508 |
| no. of data/restraints/parameters | 3237/0/255 | 4045/0/235 | 5013/3/473 | 5508/0/235 |
| goodness of fit (GOF) on F ² | 1.02 | 1.089 | 1.014 | 1.036 |
| final R indices (I > 2σ(I)) | | | | |
| R1 | 0.042 | 0.040 | 0.040 | 0.049 |
| wR2 | 0.106 | 0.111 | 0.107 | 0.121 |
| R indices (all data) | | | | |

Table 1. continued

| | AME-5 | AME-6 | AME-7 | AME-8 |
|--|--------------|--------------|--------------|-------------|
| R1 | 0.061 | 0.054 | 0.069 | 0.081 |
| wR2 | 0.118 | 0.119 | 0.092 | 0.138 |
| largest difference in peak/hole ($e \text{ \AA}^{-3}$) | 0.146/−0.184 | 0.284/−0.236 | 0.309/−0.227 | 0.399−0.350 |

package.⁵⁴ To study the strength of intramolecular hydrogen bonds and to understand the crystal packing effect, we performed structural optimization in the gas phase using the X-ray geometry as an initial model. The M06-2X/cc-pVTZ level of theory^{55,56} with the incorporation of Grimme's D3 dispersion corrections⁵⁷ was used. Vibrational frequencies were computed for the optimized structures to confirm the proper convergence to energy minima on their respective potential energy surfaces.

PIXEL Calculation. The total lattice energies and intermolecular interaction energies (E_{tot}) for dimers of AME-1–8 were calculated by the PIXEL method (in the CLP computer program package, version 12.5.2014).⁵⁸ The electron density of the molecules for PIXEL calculation has been obtained at the MP2/6-31G** level of theory by using the Gaussian16 program.⁵⁴ The total lattice energy and E_{tot} are partitioned into Coulombic (E_{Coul}), polarization (E_{pol}), dispersion (E_{disp}), and repulsion (E_{rep}) energy contributions. Further, the PIXEL interaction energies (E_{tot}) of different molecular pairs were compared with those of interaction energies (ΔE_{cp}) obtained from the DFT method at the M06-2X-D3/cc-pVTZ level of theory. The basis set superposition error (BSSE) for the interaction energies (ΔE_{cp}) was corrected using the counterpoise method.⁵⁹

Hirshfeld Surface (HS) Analysis. To characterize intermolecular interactions qualitatively and to understand the substitution effects on the crystal packing, Hirshfeld surface (HS) and decomposed 2D fingerprint (FP) plots were used. These analyses were performed with the program CrystalExplorer17.5.⁶⁰

QTAIM Analysis. Intra- and intermolecular interactions were quantified using topological properties with the AIMALL package.⁶¹ The crystal structure geometry with normalized hydrogen positions was used for this calculation at the M06-2X-D3/cc-pVTZ level of theory. The selected topological parameters such as electron density (ρ), the Laplacian of electron density ($\nabla^2\rho$), local potential energy density (V), kinetic energy density (G), and total electronic energy density ($H = V + G$) at the bond critical points (BCPs) were used to analyze these interactions. The strength of these interactions was assessed using the EML empirical formula.⁶² For all eight structures, the topological properties for various noncovalent interactions observed in different dimers and their molecular graphs are presented in the Supporting Information.

RESULTS AND DISCUSSION

General Description of the Molecular Structure and Conformation. The geminal amido esters, AME-1–8 (Scheme 1) have been synthesized from substituted anilines and diethyl ethoxymethylenemalonate (DEEMM) by using the synthesis procedures mentioned in our earlier report.⁴¹ The synthesized compounds, AME-1–8, were characterized by spectral and single-crystal X-ray diffraction studies. The ¹H NMR spectra indicate that the N–H_{amide} and N–H_{aniline} protons could be observed in the ranges of 10.80–11.23 and 12.29–12.40 ppm, respectively. In particular, this downfield shift of N–H_{aniline} might be due to the existence of an intramolecular RAHB (N1–H1_{aniline}...O1=C9_{amide}) interaction. The structures of AME-1–8 in the present study have common fragments such as an aniline ring (ring I), an anilide ring (ring II), and an ester moiety as shown in Figure 1. The vinylic double bond (C7=C8) bridges these three fragments to build the molecular structure. The molecular conformation can be described as a distorted Y-shaped conformation in which aniline and anilide moieties are oriented on opposite

sides (Figure 1). Both rings (rings I and II) are unsubstituted in AME-1, while AME-2–8 contain symmetrical substitutions (4-Me, 2-/3-/4-OMe, and 2-/3-/4-Cl) on both phenyl rings (Scheme 1 and Figure 1). All of the compounds except for AME-7 crystallize in the monoclinic crystal system with one molecule in the asymmetric unit. The compound AME-7 crystallizes in the triclinic system (in the $P\bar{1}$ space group) with two crystallographically independent molecules (molecules A and B). The crystal data and other refinement statistics are summarized in Table 1.

The phenyl ring orientations in these structures varies due to electron-withdrawing/-donating groups attached at different positions on the phenyl rings concerning the unsubstituted structure (AME-1). In the unsubstituted structure, the dihedral angle formed between the two phenyl rings is 6.98°. In the structures with an electron-donating methoxy group substituted at different positions, the corresponding angle is in the order AME-3 (24.35°) < AME-5 (17.69°) < AME-4 (10.96°). The orientation angle between two phenyl rings is greater in isotopic structures (4-Me, AME-2, 4-Cl, AME-8) and molecule B of AME-7 (3-Cl) in comparison to the other structures. The dihedral angle is in the range of 47.47–51.28°. However, the corresponding angles in 2-Cl (AME-6, 18.44°) and molecule A of AME-7 (12.33°) are similar to those of methoxy derivatives. These dihedral angles formed between different mean planes in the present work are comparable with those of amido ester structures reported earlier.⁴¹

Furthermore, the molecular twist can be measured using the two selected torsion angles C7–N1–C1–C2 (τ_1) and C9–N2–C10–C15 (τ_2) (Table S1). The molecular conformation adopts a slightly twisted conformation in some molecules in comparison to the unsubstituted molecule AME-1. The enantiomerically related molecules AME-4, AME-6, and AME-7A with respect to the unsubstituted AME-1 were used to compare these two torsion angles. This analysis suggests that the τ_1 value is in the range of 2.4–18.5° with respect to the molecule of AME-1, while the τ_2 value is in the range of 1.0–28.9°. These two torsion angles indicate that different substituents cause a twist on aryl rings to various degrees, affecting the stability of hydrogen-bridged pseudoring. The structural superposition reveals aryl ring rotation with respect to the central fragment comprising atoms H1_N/N1/C7/C8/C9/O1/N2/H2_N/C16/O2 (Figure 2). Further, we observed that two intramolecular N–H...O hydrogen bonds and a C–H...O interaction cooperatively generate three fused pseudo-6,6,6-membered rings at the center in all structures (Figures 1 and 2). These intramolecular interactions stabilize the molecular conformation. Cole and co-workers described only two intramolecular N–H...O hydrogen bonds in their study on amido ester derivatives,⁴¹ and the present study identifies an invariant weak intramolecular C–H...O interaction which also helps to lock the molecular conformation.

Resonance- and Non-Resonance-Assisted Intramolecular N–H...O Hydrogen Bonds. As was mentioned earlier, the conformation of the molecular structures AME-1–

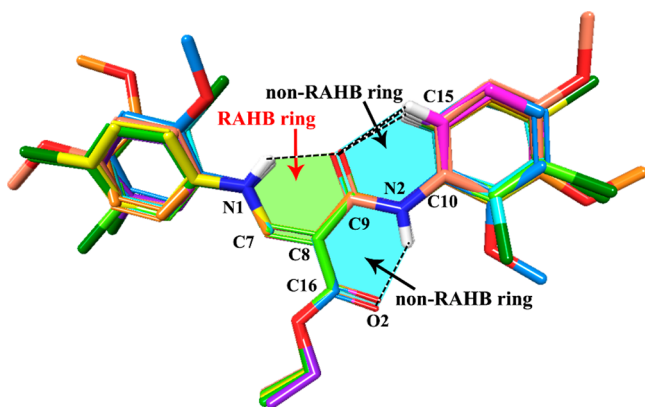


Figure 2. Structural overlay diagram for AME-1–8. Atoms used for superimposition are labeled. The RAHB ring is highlighted in yellow-green, and two non-RAHB pseudoring motifs are indicated in cyan. (color code: AME-1, magenta; AME-2, green; AME-3, blue; AME-4, orange; AME-5, violet; AME-6, cyan; AME-7A, yellow-green; AME-7B, pink; AME-8, yellow).

8 is primarily stabilized by three intramolecular N/C–H...O interactions which generate three pseudofused $S(6), S(6), S(6)$ motifs. The N–H_{aniline}, N–H_{amide}, and one of the C–H groups of ring II act as donors, and the oxygen atoms of carbonyl groups (C=O_{amide} and C=O_{ester}) act as acceptors for these interactions (Figure 1). Among three pseudofused $S(6)$ rings, one of the $S(6)$ rings (N1–H1_N...O1 or N–H_{aniline}...O=C_{amide}) is described as a resonance-assisted hydrogen-bridged (RAHB) ring on the basis of the method proposed by Gilli et al.⁹ These authors explained the λ value calculation from the bond lengths of the RAHB ring. This λ value was used to differentiate between RAHB and non-RAHB. The fully delocalized keto form of an enol ring (RAHB) has a λ value of 0.5, and a lower value of λ (in the range of 0.17–0.29) indicates a non-RAHB nature (Table S2 in the Supporting Information). Further, the hydrogen-bridged RAHB and non-RAHB rings can also be differentiated using the π -electron counts, and a greater number of π electrons is present in the RAHB ring in comparison to non-RAHB rings.

The strength and nature of the intramolecular hydrogen-bonded motifs were fully characterized by employing Bader's quantum theory of atoms in molecules (QTAIM) approach.^{42,43} Table 2 summarizes the topological parameters for intramolecular N/C–H...O interactions at the crystal structure geometry with normalized H positions. It is important to note that the strengths of the non-RAHBs, i.e., a N2–H2_N...O2 hydrogen bond, are found to be very similar in all eight structures. The dissociation energy for this hydrogen bond varies from 7.5 to 9.9 kcal mol⁻¹. The positive value of the Laplacian ($\nabla^2\rho > 0$), $H < 0$, and $| -V/G | < 1$ suggest that the non-RAHBs are closed-shell in nature (Table 3). However, the RAHB ring displays remarkable variation in the strength and nature of bonding. The dissociation energies are relatively higher in AME-1 (11.1 kcal mol⁻¹), AME-4 (11.4 kcal mol⁻¹), and AME-5 (11.3 kcal mol⁻¹) in comparison to the other structures. The positive value of the Laplacian ($\nabla^2\rho > 0$), $H > 0$, and $| -V/G | > 1$ suggest⁶³ that RAHBs in these structures show bonding character intermediate between shared and closed-shell interactions. The other substituents (4-Me, 2-OMe, 2-Cl, 3-Cl, and 4-Cl) reduce the strength of the RAHB and have relatively lower dissociation energies, varying from 6.9 to 9.4 kcal mol⁻¹. It is also noted that RAHBs

in the above five structures show closed-shell character rather than an intermediate bonding nature. Furthermore, there exists an intramolecular C–H...O interaction in which the amide carbonyl is involved as an acceptor in all structures. The strength of this weak interaction does not vary much with different substituents, as is evident from the dissociation energy (3.2–3.7 kcal mol⁻¹). As expected, this C–H...O interaction is described as a closed-shell interaction.

Further analysis suggests that an electron-withdrawing substituent (Cl) placed at different positions has an essential role in stabilizing the RAHB ring. For instance, the 4-Cl substituent deactivates the RAHB ring more than the other substituents 2-Cl and 3-Cl do. However, the 2-Cl substituent reduces the strength of the non-RAHB in comparison to 3-Cl and 4-Cl substituents. It is worth noting that an electron-donating substituent (–OMe) placed at the *ortho*, *meta*, and *para* positions shows a contrasting feature in comparison to an electron-withdrawing substituent in those different positions. The strength of the RAHB is weakened by ~ 2 kcal mol⁻¹ for 2-OMe substituent in comparison to the counterparts in *meta* and *para* positions. However, *meta* and *para* isomers of –OMe do not alter the strength of the RAHB. This variation suggests that steric and electronic effects play an essential role in the stabilization.

The intramolecular hydrogen-bonding geometries for H1...O1 (RAHB) and H2...O2 (non-RAHB) interactions are comparable with those in earlier X-ray work.⁴¹ However, the neutron diffraction studies revealed a reduction of the distance for a non-RAHB in comparison to a RAHB, but comparable distance for RAHBs in X-ray and neutron structures (unsubstituted). A contrasting feature was observed in the case of the 4-Me structure. The bond path (R_{ij}) values for H1...O1 (RAHB) derived from the QTAIM framework suggest that bond lengthening is observed in structures containing electron-withdrawing substituents in comparison to those of unsubstituted derivatives and those containing electron-donating groups. A similar trend is also noted in structures with electron-donating substituents (4-Me) and 2-OMe. In contrast, the corresponding values are comparable in structures with 3-OMe and 4-OMe groups. The values of R_{ij} and the electron density for RAHB follow the exponential decay trend with an R^2 fitting parameter value of >0.95 . A similar trend is also observed for R_{ij} and dissociation energy values, and the same is valid for non-RAHBs as well (Figures S2–S4 in the Supporting Information). However, the non-RAHBs in these structures show contracting behavior in comparison to the RAHBs. The systems with electron-withdrawing groups (3-Cl and 4-Cl) reduce the H2...O2 distance except in the 2-Cl structure. In contrast, the corresponding distance increases in unsubstituted, three-electron-donating derivatives (4-Me, 3-OMe, and 4-OMe), except for the 2-OMe derivative. Moreover, the H2...O2 distance is greater in electron-withdrawing structures than in electron-donating and unsubstituted structures. These features suggest that the amide group is more acidic in electron-withdrawing structures than in electron-donating derivatives.

In order to understand the role of crystal packing on the strength and nature of the RAHB and the non-RAHB, we performed a topological analysis for optimized structures as well. The selected topological parameters for these intramolecular interactions in gas-phase optimized structures are given in Table S3. The molecular graphs showing the existence of these intramolecular interactions are depicted in Figure S1.

Table 2. Topological Parameters for Intramolecular Interactions Observed in AME-1–8^a

| atoms | R_{ij} | ρ | $\nabla^2\rho$ | V | G | H | DE_{int} | $\left \frac{-V}{G}\right $ |
|-----------|----------|--------|----------------|---------|--------|-------------------|-------------|-----------------------------|
| AME-1 | | | | | | | | |
| NIH1...O1 | 1.853 | 0.2494 | 3.2112 | -0.0353 | 0.0343 | 0.0010 (0.0015) | 11.1 (11.6) | 1.03 (1.04) |
| N2H2...O2 | 1.938 | 0.2037 | 3.1820 | -0.0284 | 0.0307 | -0.0023 (0.0010) | 8.9 (10.7) | 0.92 (1.03) |
| H15...O1 | 2.424 | 0.0986 | 1.5522 | -0.0104 | 0.0133 | -0.0029 (-0.0034) | 3.3 (4.1) | 0.78 (0.79) |
| AME-3 | | | | | | | | |
| NIH1...O1 | 1.940 | 0.2116 | 3.4342 | -0.0299 | 0.0327 | -0.0029 (0.0000) | 9.4 (10.6) | 0.91 (1.00) |
| N2H2...O2 | 1.926 | 0.2069 | 3.2571 | -0.0294 | 0.0316 | -0.0022 (-0.0003) | 9.2 (9.7) | 0.93 (0.99) |
| H15...O1 | 2.336 | 0.1100 | 1.7651 | -0.0118 | 0.0151 | -0.0033 (-0.0035) | 3.7 (4.2) | 0.78 (0.79) |
| AME-4 | | | | | | | | |
| NIH1...O1 | 1.850 | 0.2496 | 3.2970 | -0.0364 | 0.0353 | 0.0011 (0.0014) | 11.4 (11.6) | 1.03 (1.04) |
| N2H2...O2 | 1.906 | 0.2188 | 3.3457 | -0.0315 | 0.0331 | -0.0016 (0.0010) | 9.9 (10.7) | 0.95 (1.03) |
| H15...O1 | 2.381 | 0.1008 | 1.5984 | -0.0106 | 0.0136 | -0.0030 (-0.0034) | 3.3 (4.1) | 0.78 (0.79) |
| AME-5 | | | | | | | | |
| NIH1...O1 | 1.853 | 0.2512 | 3.3827 | -0.0362 | 0.0356 | 0.0005 (0.0015) | 11.4 (11.7) | 1.02 (1.04) |
| N2H2...O2 | 1.952 | 0.1955 | 3.0092 | -0.0267 | 0.0289 | -0.0023 (0.0009) | 8.4 (10.6) | 0.92 (1.03) |
| H15...O1 | 2.348 | 0.1101 | 1.7702 | -0.0119 | 0.0151 | -0.0032 (-0.0034) | 3.7 (4.1) | 0.79 (0.79) |
| AME-6 | | | | | | | | |
| NIH1...O1 | 1.984 | 0.1913 | 3.2258 | -0.0263 | 0.0299 | -0.0036 (0.0010) | 8.2 (11.4) | 0.88 (1.03) |
| N2H2...O2 | 2.008 | 0.1757 | 3.0282 | -0.0240 | 0.0277 | -0.0037 (0.0005) | 7.5 (10.3) | 0.87 (1.02) |
| H15...O1 | 2.417 | 0.1023 | 1.6191 | -0.0109 | 0.0139 | -0.0029 (-0.0036) | 3.4 (4.7) | 0.79 (0.80) |
| AME-7A | | | | | | | | |
| NIH1...O1 | 2.023 | 0.1793 | 3.0164 | -0.0234 | 0.0274 | -0.0039 (0.0015) | 7.4 (11.7) | 0.86 (1.04) |
| N2H2...O2 | 1.968 | 0.1925 | 3.1258 | -0.0263 | 0.0294 | -0.0031 (0.0014) | 8.3 (11.0) | 0.90 (1.04) |
| H15...O1 | 2.425 | 0.0995 | 1.5637 | -0.0105 | 0.0134 | -0.0029 (-0.0035) | 3.3 (4.2) | 0.79 (0.79) |
| AME-7B | | | | | | | | |
| NIH1...O1 | 2.012 | 0.1858 | 3.1695 | -0.0248 | 0.0288 | -0.0041 (0.0015) | 7.8 (11.7) | 0.86 (1.04) |
| N2H2...O2 | 1.970 | 0.1921 | 3.1268 | -0.0262 | 0.0293 | -0.0031 (0.0014) | 8.2 (11.0) | 0.89 (1.04) |
| H15...O1 | 2.362 | 0.1054 | 1.6830 | -0.0112 | 0.0143 | -0.0031 (-0.0034) | 3.5 (4.1) | 0.78 (0.79) |
| AME-2 | | | | | | | | |
| NIH1...O1 | 1.925 | 0.2135 | 3.1746 | -0.0291 | 0.0310 | -0.0019 (0.0015) | 9.1 (11.7) | 0.94 (1.04) |
| N2H2...O2 | 1.957 | 0.1949 | 3.0804 | -0.0267 | 0.0293 | -0.0026 (0.0009) | 8.4 (10.6) | 0.91 (1.03) |
| H15...O1 | 2.404 | 0.0974 | 1.5295 | -0.0101 | 0.0130 | -0.0029 (-0.0034) | 3.2 (4.1) | 0.78 (0.79) |
| AME-8 | | | | | | | | |
| NIH1...O1 | 2.051 | 0.1693 | 2.9577 | -0.0221 | 0.0264 | -0.0043 (0.0015) | 6.9 (11.7) | 0.84 (1.04) |
| N2H2...O2 | 1.951 | 0.1991 | 3.1954 | -0.0277 | 0.0304 | -0.0027 (0.0013) | 8.7 (10.9) | 0.91 (1.04) |
| H15...O1 | 2.364 | 0.1038 | 1.6483 | -0.0109 | 0.0140 | -0.0031 (-0.0035) | 3.4 (4.2) | 0.78 (0.79) |

^aX-ray geometry with normalized H positions. Definitions: R_{ij} , Bond path (Å); ρ , electron density ($e \text{ \AA}^{-3}$); $\nabla^2\rho$, Laplacian electron density ($e \text{ \AA}^{-5}$); V , potential energy density; G , kinetic energy density; H , total electronic density; DE_{int} , dissociation energy = $-V \times 0.5 \text{ kcal mol}^{-1}$. The values of V , G , and H are expressed in au. The values in parentheses correspond to optimized structures.

In the isolated molecules, the bond path values for H1...O1 and H2...O2 interactions are significantly reduced in both electron-donating and electron-withdrawing derivatives in comparison to the X-ray structures and there is a marginal variation in the unsubstituted structure. This reduction in the bond path values for both RAHBs and non-RAHBs and the strength and nature of these bonds are very similar irrespective of donating and withdrawing groups. These data clearly support that crystal packing modulates the strength and nature of both RAHB and non-RAHB motifs but has a pronounced effect on the RAHB motif.

PIXEL Energy Analysis: Intermolecular Interaction Energies. PIXEL calculations were performed to identify energetically significant dimers from the crystal structures of AME-1–8. The interaction geometries and the interaction energies for dimers computed by two different approximations (M06-2X and MP2) are given in Table 3. The complete information, including the different energy components of total intermolecular interactions for dimers, is summarized in Table S5. We found that the intermolecular interaction energies for

the weak dimers in these structures, which are calculated from the PIXEL (E_{tot}) and the counterpoise (ΔE_{cp}) methods, are comparable. However, for the strongest dimers formed by resonance-assisted ring-stacking interactions, the interaction energies are overestimated by the M06-2X-D3/cc-pVTZ level in comparison to the MP2/6-31G** level of theory. This overestimation could be due to the dispersion energy and the type of interactions present in them. As was mentioned earlier, two crystallographically independent molecules (molecules A and B) exist in the asymmetric unit of AME-7. The dimers formed between molecule A and its symmetry-related partners (A...A), molecule B and its symmetry-related partners (B...B), and between molecules of A and B (B...A/B...A) are considered separately. For clarity, we included labels for interacting molecules such as AA, BB, and AB with dimeric motif numbers (Table 3 and Table S5). As amine groups are engaged in intramolecular N–H...O hydrogen bonds with carbonyl oxygens, the crystal structures of AME-1–8 are stabilized by several weak C–H...O, C–H... π , C–H...Cl, and π ... π interactions. However, one of the amine groups is

Table 3. Intermolecular Interaction Energies (in kcal mol⁻¹) for Various Dimers in AME1–8^{af}

| dimer | CD | symmetry code | possible interactions | geometry H...A (Å), ∠(D–H...A) (deg) ^b | E _{tot} ^c | ΔE _{cp} ^d |
|----------------|--------|------------------------------|---|---|-------------------------------|-------------------------------|
| AME-1 | | | | | | |
| D ₁ | 3.087 | -x, 1 - y, -z | C7...C9 C _{GRAHB} ...C _{GRAHB} | 3.336(2) 3.608 | -15.3 | -21.0 |
| D ₂ | 4.461 | 1 - x, 1 - y, -z | C18–H18C...Cg2 (π) C9...C16 | 3.00, 158 3.437(2) | -13.3 | -15.7 |
| D ₃ | 10.185 | -x, -1/2 + y, -1/2 - z | C5–H5...O1=C9 | 2.62, 136 | -4.5 | -3.3 |
| D ₄ | 12.320 | 1 - x, 1/2 + y, 1/2 - z | C12–H12...O2=C16 | 2.58, 153 | -2.2 | -1.9 |
| AME-2 | | | | | | |
| D ₁ | 3.334 | -x, 1 - y, -z | C2–H2...O2=C16 C7...N2 C8...C8 C11–H11...Cg1 C _{GRAHB} ...C _{GRAHB} | 2.75, 118 3.298(2) 3.425(2) 2.71, 138 3.943 | -16.9 | -22.5 |
| D ₂ | 5.447 | -x, y, 1/2-z | C6–H6...O1=C9 C6–H6... C _{GRAHB} | 2.79, 119 2.59, 131 | -11.6 | -12.6 |
| D ₃ | 9.507 | 1/2 - x, 1/2 - y, -z | C14–H14...O1=C9 C14–H14...H15–C15 | 2.54, 169 2.372(1) | -5.8 | -4.9 |
| D ₄ | 10.983 | 1/2 - x, 3/2 - y, -z | C12–H12...O2=C16 | 2.59, 137 | -5.4 | -4.6 |
| D ₅ | 11.148 | x - 1/2, y - 1/2, -z | C3–H3...Cg2 (C14) | 2.55, 134 | -4.8 | -6.0 |
| D ₆ | 13.250 | x - 1/2, -y + 1/2, z + 1/2 | C19–H19A...Cg2 (C13) | 2.70, 152 | -4.0 | -5.2 |
| AME-3 | | | | | | |
| D ₁ | 5.264 | 1 - x, -y, -z | C8...C16 C17–H17B...O1=C9 | 3.419(2) 2.81, 122 | -15.2 | -18.3 |
| D ₂ | 9.141 | 1 - x, -y, 1 - z | C19–H19B...O1=C9 | 2.54, 131 | -10.2 | -9.0 |
| D ₃ | 8.951 | -1/2 + x, 1/2 - y, -1/2 + z | C9 = O1...C20 C20–H20C...O4 | 3.022(2) 2.58, 160 | -5.7 | -6.1 |
| D ₄ | 11.043 | 2 - x, -y, 1 - z | C19–H19A...Cg1(C5) | 3.05, 145 | -4.9 | -6.1 |
| D ₅ | 9.453 | 3/2 - x, -1/2 + y, 1/2 - z | C4–H4...O5 | 2.68, 146 | -4.6 | -4.5 |
| D ₆ | 9.069 | 1 + x, y, z | C18–H18A...C11 | 2.87, 138 | -3.7 | -4.4 |
| D ₇ | 11.334 | 2 - x, -y, -z | C18–H18B...C6 | 2.84, 143 | -3.2 | -2.3 |
| AME-4 | | | | | | |
| D ₁ | 4.269 | x, -y + 1/2, z + 1/2 | C _{GRAHB} ...C _{GRAHB} C17–H17B...C15 C17–H17A...Cg2 | 4.068 2.82, 137 3.25, 117 | -14.4 | -17.7 |
| D ₂ | 8.146 | 1 - x, 1 - y, -z | C2–H2...H13–C13 C20–H20C...O4 C14–H14...O1=C9 | 2.304 2.82, 121 2.78, 153 | -7.5 | -5.6 |
| D ₃ | 13.697 | 1 + x, 1/2 - y, -1/2 + z | C19–H19B...O2=C16 | 2.61, 100 | -4.8 | -4.2 |
| D ₄ | 14.361 | -x, 1 - y, -z | C20–H20C...C12 | 2.89, 131 | -3.9 | -4.6 |
| D ₅ | 11.925 | 1 - x, -y, -z | C18–H18B...C6 | 3.02, 135 | -2.2 | -1.4 |
| AME-5 | | | | | | |
| D ₁ | 3.489 | -x, -y, -z | C _{GRAHB} ...C _{GRAHB} | 3.832 | -15.7 | -19.4 |
| D ₂ | 5.284 | -x, y, -z + 1/2 | C7...C7 | 4.494(3) | -13.0 | -15.2 |
| D ₃ | 10.449 | 1/2 - x, -1/2 + y, 1/2 - z | C2–H2...O5 C12–H12...O1=C9 C20–H20A...O2=C16 C20–H20B...C2 | 261, 129 2.52, 176 2.62, 131 2.84, 124 | -6.8 | -5.7 |
| D ₄ | 11.120 | x - 1/2, -y - 1/2, z - 1/2 | C19–H19C...O1=C9 | 2.76, 131 | -5.4 | -6.5 |
| D ₅ | 13.838 | x + 1/2, y + 1/2, z | C20–H20C...O4 C19–H19B...Cg2 (C14) | 2.65, 143 2.75, 161 | -4.9 | -6.1 |
| D ₆ | 12.497 | x, y+1, z | C18–H18B...O4 | 2.51, 159 | -2.1 | -1.6 |
| AME-6 | | | | | | |
| D ₁ | 3.354 | -x, -y, 1 - z | C _{GRAHB} ...C _{GRAHB} C7...C9 C8...C9 | 3.712 3.343(2) 3.415(2) | -17.8 | -21.9 |
| D ₂ | 5.474 | -x, -1 - y, 1 - z | C1...C8 C6...C9 | 3.487(2) 3.464(2) | -15.6 | -17.8 |
| D ₃ | 9.647 | 1/2 - x, -1/2 + y, 3/2 - z | C13–H13...O1=C9 C13–H13...Cl1 | 2.50, 132 2.93, 122 | -4.6 | -3.9 |
| D ₄ | 10.948 | -1/2 + x, -1/2 - y, 1/2 + z | C3–H3...O2=C16 | 2.53, 144 | -3.8 | -3.3 |
| D ₅ | 10.621 | -1/2 + x, -1/2 - y, -1/2 + z | C18–H18A...Cg2 | 3.07, 142 | -2.9 | -3.0 |

Table 3. continued

| dimer | CD | symmetry code | possible interactions | geometry H...A (Å), ∠(D-H...A) (deg) ^b | E_{tot} ^c | ΔE_{cp} ^d |
|------------------|--------|----------------------------|--|---|-------------------------------|-------------------------------------|
| AME-6 | | | | | | |
| D ₆ | 10.892 | 1/2 - x, -1/2 + y, 1/2 - z | C17-H17A...Cl2 | 2.95, 136 | -2.5 | -1.9 |
| AME-7 | | | | | | |
| D _{1BB} | 3.600 | 2 - x, 2 - y, -z | C28...C29 | 3.356 | -17.9 | -21.0 |
| | | | C _{GRAHB} ...C _{GRAHB} | 4.067 | | |
| | | | C28...C28 | 3.433(4) | | |
| D _{2AA} | 3.438 | 1 - x, 1 - y, 1 - z | C31-H31...C26(Cg1B) | 3.11, 130 | -17.3 | -21.4 |
| | | | C8...C9 | 3.517(5) | | |
| | | | C _{GRAHB} ...C _{GRAHB} | 3.876 | | |
| D _{3AA} | 4.456 | 2 - x, 1 - y, 1 - z | C1...C9 | 3.402(5) | -14.3 | -18.3 |
| | | | C _{GRAHB} ...C _{GRAHB} | 3.590 | | |
| D _{4BB} | 4.795 | 1 - x, 2 - y, -z | C22-H22...O5=C36 | 2.51, 135 | -13.3 | -12.8 |
| D _{5AB} | 10.482 | 1 - x, 2 - y, 1 - z | C29=O4...Cl2 | 3.220(2) | -6.8 | -5.8 |
| | | | N3-H3 _N ...Cl2 | 2.85, 142 | | |
| | | | C11-H11...C26 | 2.87, 153 | | |
| | | | C24-H24...O2=C16 | 2.79, 111 | | |
| D _{6AB} | 10.728 | -2x, 2 - y, -z | C18-H18B...Cg2B | 2.69, 162 | -4.9 | -4.6 |
| D _{7AB} | 11.008 | x, y, z | C17-H17A...Cl3 | 3.04, 114 | -3.5 | -2.5 |
| D _{8BB} | 17.084 | -1+x, y, 1+z | Cl3...Cl4 | 3.492(1) | -1.0 | -0.7 |
| AME-8 | | | | | | |
| D ₁ | 3.573 | -x, 1 - y, -z | C2-H2...O2=C16 | 2.75, 113 | -17.9 | -22.0 |
| | | | C _{GRAHB} ...C _{GRAHB} | 4.073 | | |
| | | | C8...C8 | 3.472(2) | | |
| | | | C11-H11...Cg1 | 2.75, 137 | | |
| D ₂ | 5.727 | -x, y, 1/2 - z | C6-H6...O1 = C9 | 2.86, 118 | -10.9 | -11.7 |
| | | | C6-H6... C _{GRAHB} | 2.66, 130 | | |
| D ₃ | 8.882 | 3/2 - x, 1/2 - y, -z | C14-H14...O1=C9 | 2.40, 175 | -9.8 | -7.5 |
| D ₄ | 11.053 | 3/2 - x, 3/2 - y, -z | C12-H12...O2=C16 | 2.54, 136 | -6.8 | -5.0 |
| D ₅ | 11.092 | -1/2 + x, -1/2 + y, z | C3-H3...Cg2 | 2.61, 131 | -4.6 | -5.3 |
| D ₆ | 12.906 | -1/2 + x, 1/2 - y, 1/2 + z | Cl1...Cg2 | 3.857(1) | -3.3 | -2.0 |

^aDefinitions: CD, the centroid-centroid distance of the molecules in Å; C_{GRAHB}: the center of gravity for the RAHB ring (N1-H1_N...O1/C9/C8/C7); Cg1 and Cg2, the centers of gravity for the phenyl rings C1-C6 (ring I) and C10-C15 (ring II), respectively. ^bNeutron values are given for all D-H...A interactions. ^cPIXEL interaction energies. ^d ΔE_{cp} obtained from the DFT calculations at the M06-2X/cc-pVTZ level of theory.

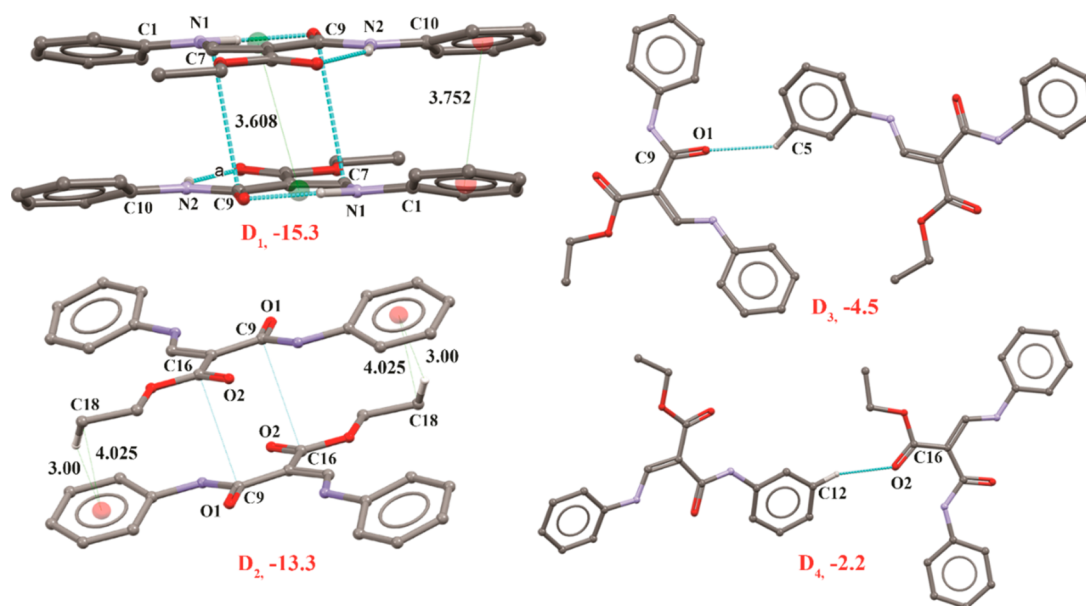


Figure 3. Selected molecular dimers in AME-1 along with E_{tot} values in kcal mol⁻¹ (see Table 3).

engaged in the intermolecular N-H...Cl hydrogen bond in AME-7. The common packing features in AME-1-8 are discussed in a separate section. A detailed qualitative analysis

of various intermolecular interactions existing in AME-1-8 with Hirshfeld surface (HS) and 2D fingerprint plots (2D-FP) is summarized in Figures S5-S7 in the Supporting

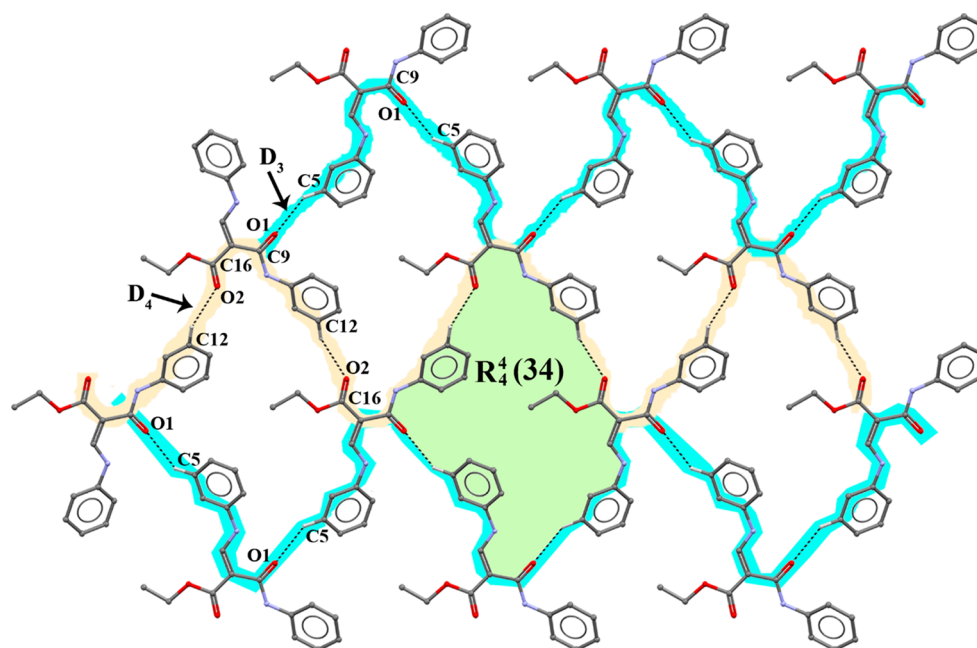


Figure 4. Part of the crystal structure of AME-1, viewed down the a axis. H atoms not involved in the C–H...O interactions are omitted. The two individual C(9) molecular chains traced with different colors and the $R_4^1(34)$ motif formed by C–H...O interactions in D_3 and D_4 are also shown.

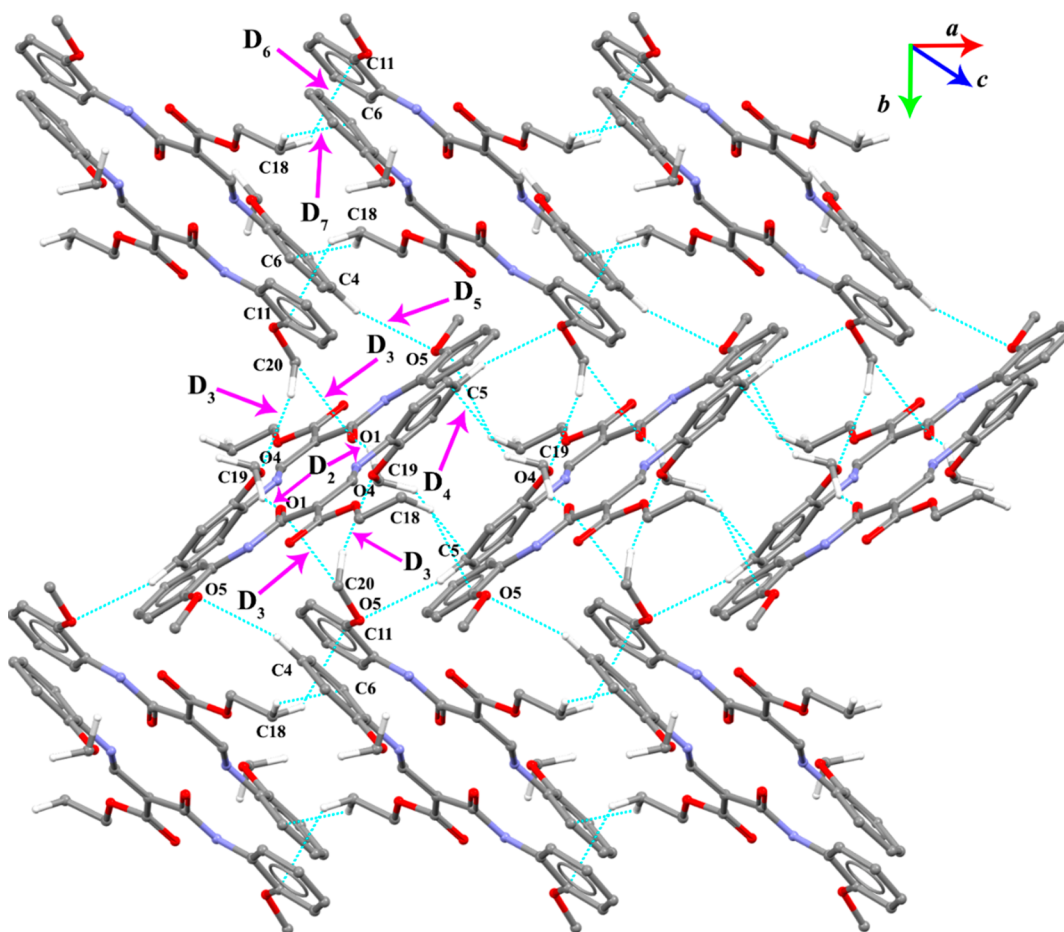


Figure 5. Various C–H...O/C and C...O interactions forming a herringbone architecture in AME-3.

Information. Further, the quantitative molecular electrostatic potential (MESP) analysis is presented in the ESI section (Figure S8).

Intermolecular Interactions in AME-1. Molecules of AME-1 form as layers along the crystallographic ac plane, and these layers are further interconnected by a stacking (dimer

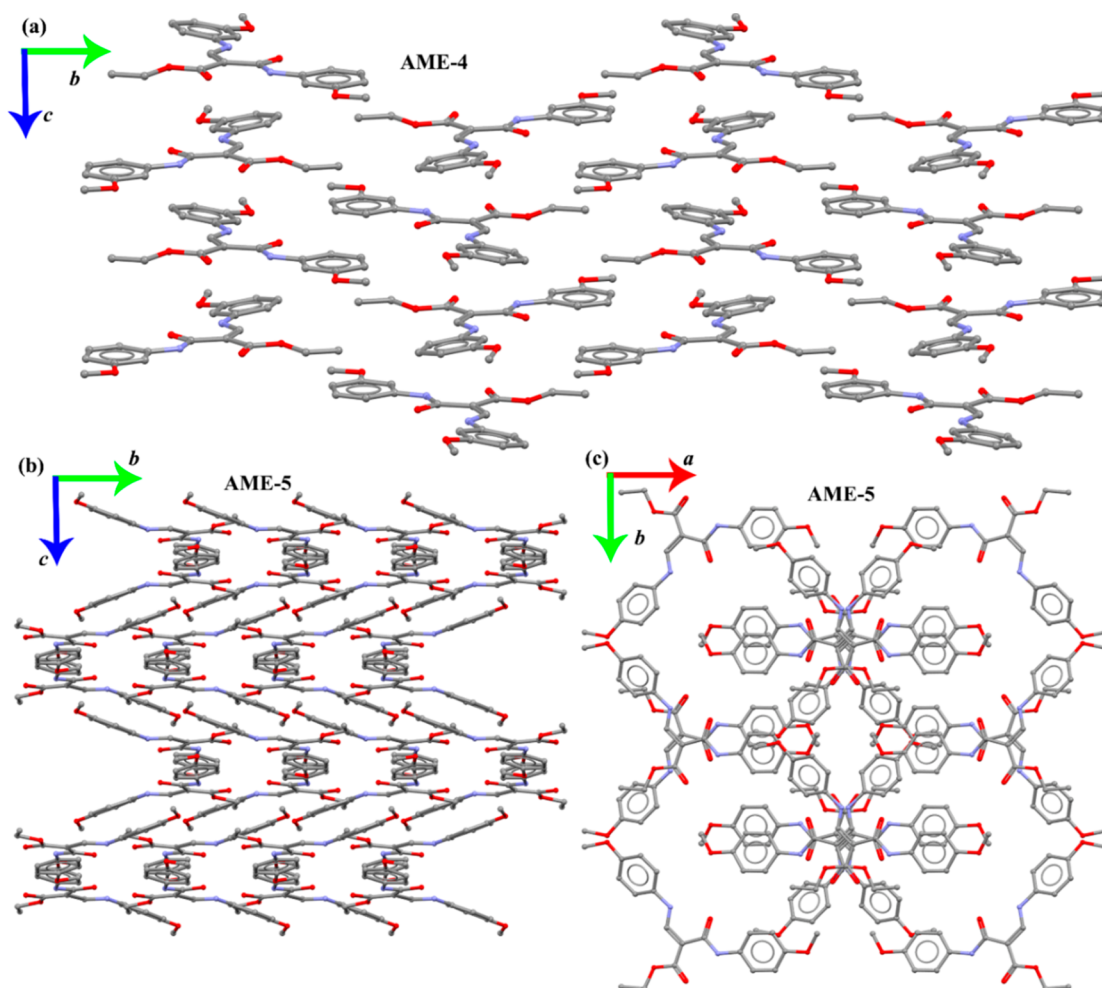


Figure 6. Packing diagrams of AME-4 and AME-5.

D_1) interaction in which adjacent resonance-assisted pseudoring are involved in the π -stacking interaction. A similar kind of interaction between two resonance-assisted hydrogen-bridged rings has been reported.^{64–68} Blagojević and Zarić have performed a systematic analysis to compute stacked hydrogen-bridged ring stabilization energies.⁶⁴ The stacking interactions occurred in different systems were analyzed, for example, between non-RAHB rings (particularly (i) two planar five-membered hydrogen-bridged rings⁶⁴ and (ii) planar six-membered hydrogen-bridged rings and C_6 -aromatic rings⁶⁹) and RAHB rings ((iii) two six-membered RAHB rings⁷⁰ and (iv) six-membered RAHB rings and C_6 -aromatic rings⁷¹). In these studies, the authors demonstrated that the stacking interactions between two six-membered RAHB rings (-4.7 kcal mol⁻¹) and the stacking interaction between the six-membered RAHB ring and C_6 -aromatic rings (-3.7 kcal mol⁻¹) were more robust than the normal benzene \cdots benzene stacking interaction (-2.7 kcal mol⁻¹).⁷¹ In the present work, we did not observe any stacking interactions between aromatic rings or between aromatic and hydrogen-bridged pseudoring. The PIXEL energy analysis revealed that there are four energetically significant intermolecular dimers (D_1 – D_4) identified from the crystal packing. The intermolecular interaction energies (E_{tot}) range from -15.3 to -2.2 kcal mol⁻¹ (Table 3 and Figure 3). In all four dimers, dispersion energies contribute more than two thirds of their stabilization energies (Table S5). We note that the dimer D_2 also forms by

$C9\cdots C16$ ($\pi\cdots\pi$) contacts and is further supported by an intermolecular $C-H\cdots\pi$ (involving H18C and Cg2) interaction with an E_{tot} value of -13.3 kcal mol⁻¹.

The O1 and O2 atoms of carbonyl units ($C=O_{amide}$ and $C=O_{ester}$) are involved in intermolecular $C-H\cdots O$ interactions ($C5-H5\cdots O1=C9$, $D3$, $E_{tot} = -4.5$ kcal mol⁻¹; $C12-H12\cdots O2=C16$, $D4$, $E_{tot} = -2.2$ kcal mol⁻¹). Each of these interactions link the molecules into a $C(9)$ chain, and these chains run parallel to each other. When these two interactions are combined, a tetrameric supramolecular sheet with the $R_4^2(34)$ motif is formed, as shown in Figure 4.

Intermolecular Interactions in Methoxy-Substituted Isomers (AME-3–5). In the crystalline state, molecules of 3-OMe (AME-4) and 4-OMe (AME-5) pack somewhat similarly and these two molecules form as layers. The basic motif formed in 2-OMe (AME-3) is the stacking between adjacent molecules (D_1). This stacking motif is different from the stacking of resonance-assisted rings observed in AME-1. The basic dimeric motif in AME-3 is repeated along the b axis and form as columns. The molecules in adjacent columns generate a herringbone-like supramolecular architecture. In Table 3 and Figures S10–S12, the important dimers observed in these isomers are summarized. In all three isomers, the strong dimer is formed by stacking interactions. However, molecular stacking is different in AME-3 in comparison to AME-4 and AME-5. In the last two structures, molecular stacking is achieved by an adjacent intramolecular resonance-assisted

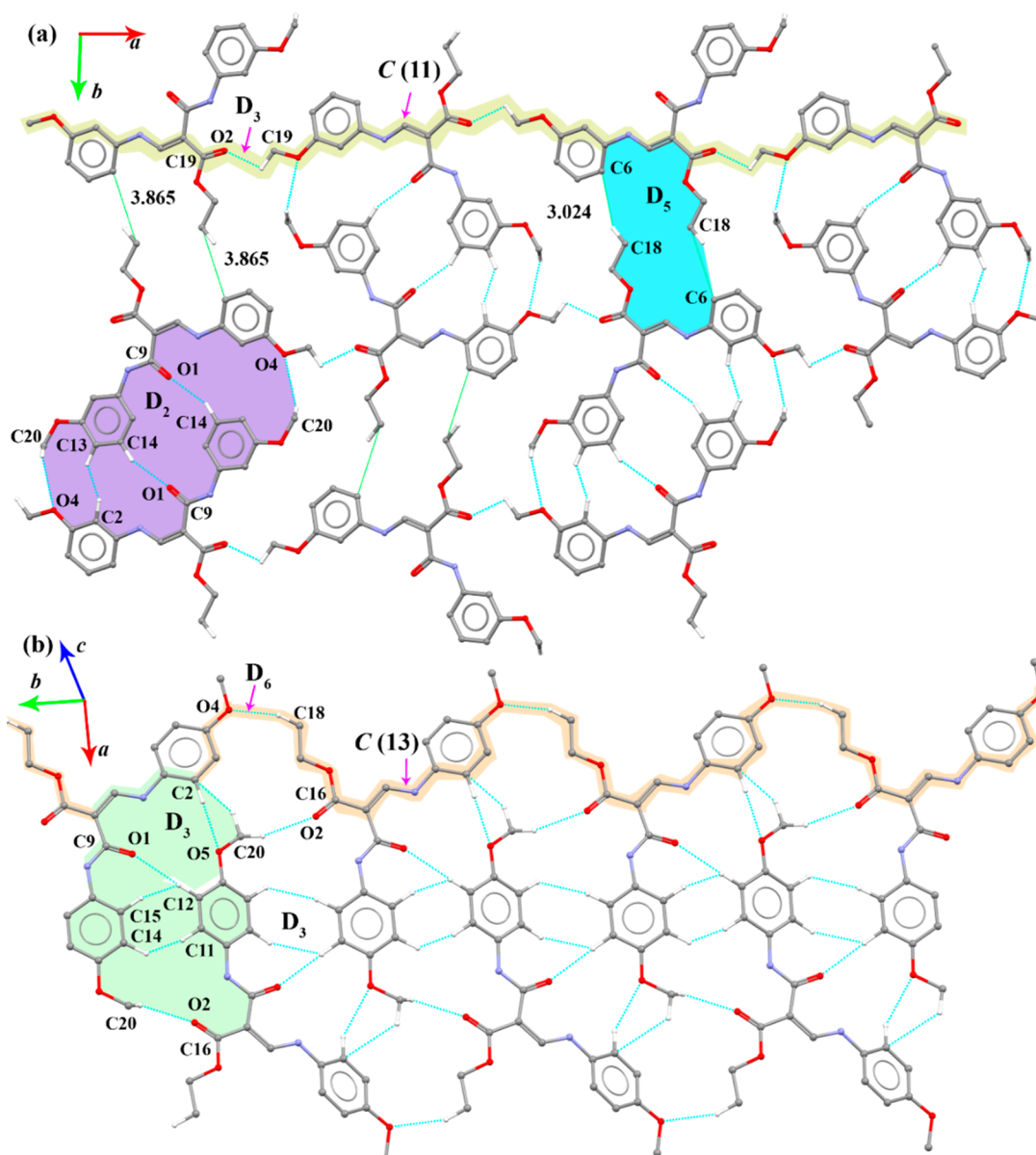


Figure 7. (a) C–H···O/C interactions in D₂, D₃, and D₅ forming a supramolecular sheet in AME-4. (b) C–H···O interactions in D₂ and D₆ forming a supramolecular sheet in AME-5.

hydrogen-bridged six-membered ring. However, there are no stacking interactions observed between the aromatic rings (rings I and II) in AME-4 and AME-5.

In AME-3, both methoxy methyl (C19 and C20) groups are involved in the intermolecular C–H···O interactions (D₂ and D₃). In one of the C–H···O interactions, molecules of AME-3 form a closed motif (D₂). This D₂ dimer is flanked on both sides by dimer D₃. The dimer D₃ is also supported by a C=O···C (involving O1 and C20) contact in addition to a C–H···O interaction. Interactions formed in D₂ and D₃ dimers act together to link the adjacent columns, which in turn produce a herringbone architecture (Figure 5).

The dimer D₄ is stabilized by an intermolecular C–H···π (involving H19A and the centroid of Cg1) interaction, and this interaction helps to link the adjacent basic motifs (D₁) arranged in each column. Further, intermolecular C4–H4···O5 (D₅), C18–H18A···C11 (D₆), and C18–H18B···C6 interactions (D₇) also stabilize the herringbone architecture. It is noted that an H4···O5 contact is established with the sum of

vdW radii + 0.1 Å. The E_{tot} values for dimers D₁–D₇ fall in the range of -15.2 to -3.2 kcal mol⁻¹ (Table 3 and Figure S10). All seven dimeric pairs are observed in AME-3 except for D₂ and D₃; the dispersion energies contribute more than 70% toward the stabilization.

In AME-4, there are five dimers (D₁–D₅; $-14.4 < E_{\text{tot}} > -2.2$ kcal mol⁻¹; Figure S11) identified from the PIXEL energy analysis. The molecules are packed as helical-like chains which run parallel to the crystallographic *b* axis or form as layers along the *ac* plane (Figure 6a). As was noted earlier, the strong dimer (D₁) forms by stacking between resonance-assisted rings of adjacent molecules in an offset mode, with the separation between them being 4.06 Å. Further stabilization is achieved by intermolecular C–H···π interactions (the CH₂ group of the ester moiety is involved as a donor). The dimer D₁ acts as a basic motif. Dimer D₂ is stabilized by two weak intermolecular C–H···O interactions and a short H···H contact forming a closed molecular loop.

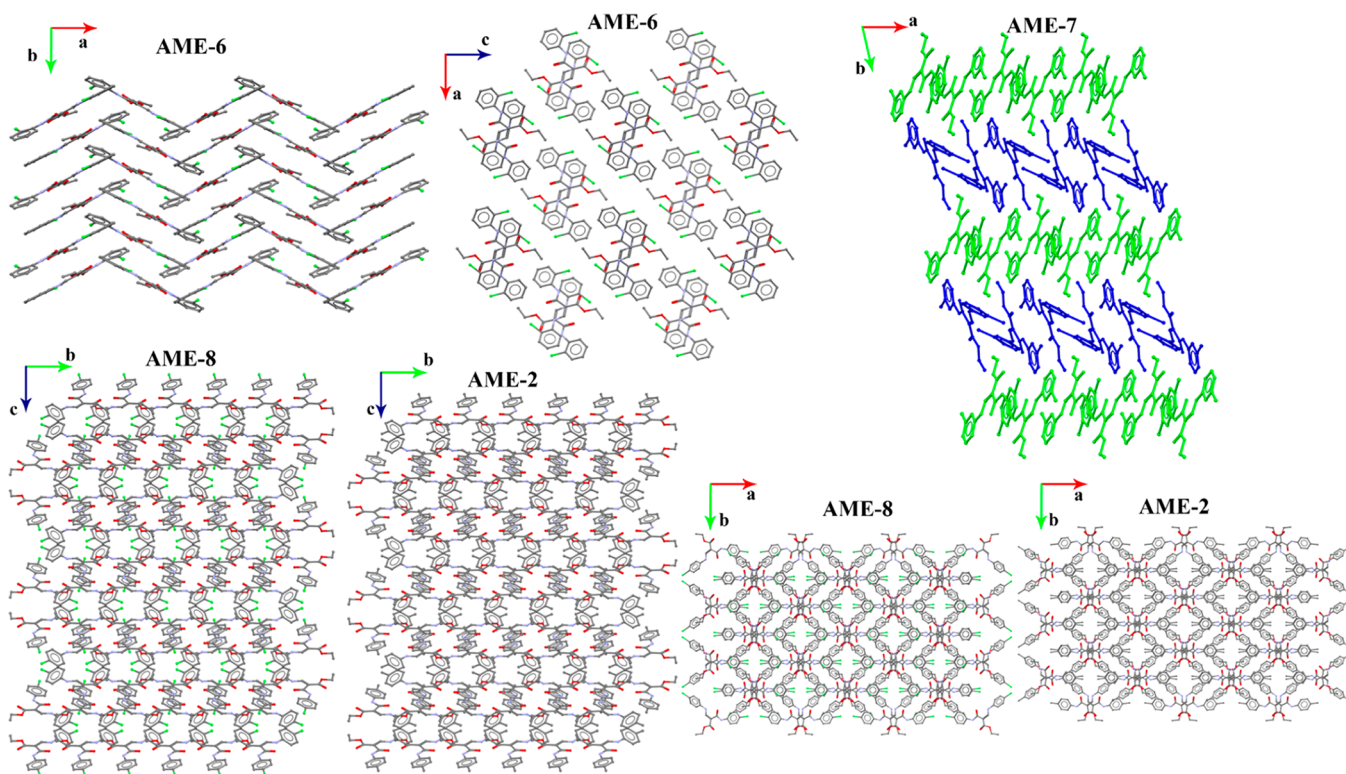


Figure 8. Crystal packing of chloro-substituted isomers AME-6–8 and of AME-2.

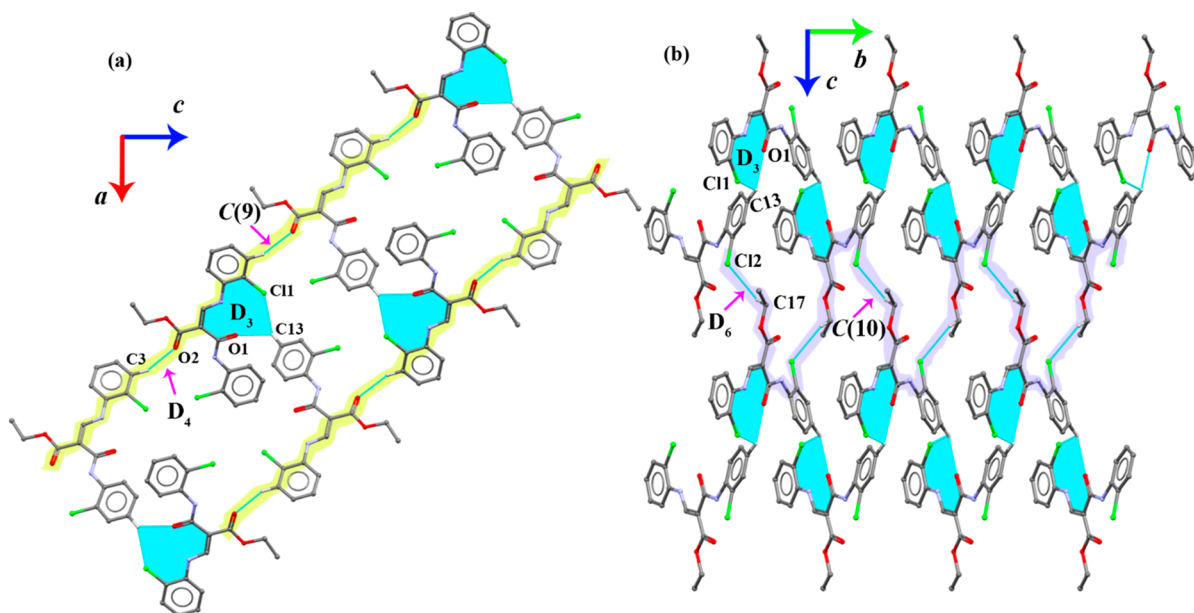


Figure 9. Part of the crystal structure in AME-6: (a) C–H...O/Cl interactions in D_3 and D_4 forming the molecular layers (ladderlike); (b) C–H...Cl (D_6) interactions linking the neighboring basic pattern of AME-6 into a herringbone architecture. Different molecular chains are highlighted.

For the C–H...O interactions, amide C=O (O1) and oxygen (O4) of the methoxy group are involved as acceptors. Similarly, dimer D_3 is also stabilized by a weak C–H...O interaction (involving H19B and O2), which links the molecules into a C(11) chain that runs parallel to the a axis. As shown in Figure 7a, dimers D_2 , D_3 , and D_5 collectively generate a supramolecular sheet. The dimer D_4 in this structure is formed by a C20–H20C...C12 interaction. This interaction links the molecules in the adjacent layers. For all four dimers observed in this structure, the contribution of

dispersion energy ranges from 60 to 79% toward the stabilization.

In AME-5, there are six dimers formed (D_1 – D_6 ; $-15.7 < E_{\text{tot}} > -2.1$ kcal mol $^{-1}$; Figure S12) in the crystal structure, as revealed by the PIXEL energy analysis. As was mentioned earlier, AME-4 and AME-5 show somewhat similar crystal packings. The AME-4 molecules packed as a single helical-like chain, whereas molecules of AME-5 form as double-helical-like chains which run in the opposite direction along the ab plane (Figure 6) or layers along the ac plane. The basic motif is

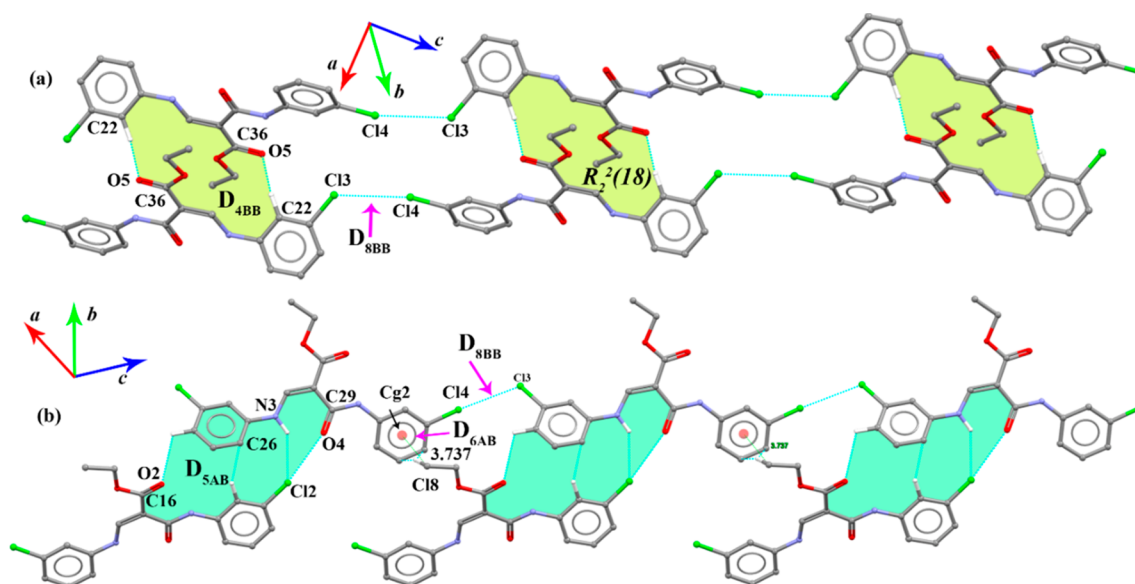


Figure 10. Part of the crystal structure of AME-7: (a) C–H...O and Cl...Cl interactions in D_{4BB} and D_{8BB} generating the molecular ribbon; (b) C–H...O/C/Cl and Cl...Cl/O interactions in D_{5AB} , D_{6AB} , and D_{8BB} generating the molecular ribbon.

derived from resonance-assisted stacking between adjacent inversion-related molecules of AME-5 (D_1). The remaining dimers are primarily stabilized with intermolecular C–H...O interactions. The oxygens (O1 and O2) of C=O groups and oxygens (O4 and O5) of methoxy groups participate as acceptors for these C–H...O interactions. The dimer D_2 is generated by molecular stacking in which the shortest distance between two adjacent C7 atoms is 3.494(3) Å. The C–H...O interactions in D_3 (C2–H2...O5, C12–H12...O1=C9, and C20–H20A...O2=C16) link the neighboring molecules into a chain which runs parallel to the *b* axis. This dimeric motif forms by D_6 (C18–H18B...O4 interaction) generating a supramolecular sheet along the *ab* plane (Figure 7b). Further, molecules in the helical-like chain are interlinked via C19–H19C...O1=C9 (D_4) and C20–H20C...O4 and C19–H19B... π (D_5) interactions (Figure 6).

Intermolecular Interactions in Chloro-Substituted Isomers (AME-6–8) and Isomorphous Forms of 4-Cl (AME-8) and 4-Me Derivatives (AME-2). In AME-6, there are six dimers (D_1 – D_6 ; $-17.8 < E_{\text{tot}} > -2.5$ kcal mol⁻¹; Figure S13) extracted from the crystal structure. The crystal packing of this structure can be described as a herringbone architecture along the *ab* plane (Figure 8). The basic pattern (D_1) observed is the stacking of resonance-assisted rings, as observed in other structures in the present study. Dimer D_2 also formed by molecular stacking in an offset mode. The shortest C...C (C1...C8 = 3.487(2) Å and C6...C9 = 3.464(2) Å) contacts are observed within this dimer. Further, dimers D_1 and D_2 are alternately arranged and one molecule from each dimer participates in the formation of dimers D_1 and D_2 . Both carbonyl oxygens (O1 and O2) are involved as acceptors for two different intermolecular C–H...O interactions, generating dimers D_3 ($E_{\text{tot}} = -4.6$ kcal mol⁻¹) and D_4 ($E_{\text{tot}} = -3.8$ kcal mol⁻¹).

The dimers D_4 are also supported by a weak intermolecular C–H...Cl contact (involving H13 and Cl1), forming a three-centered interaction. It is noted that the interactions in D_3 and D_4 interlink the basic pattern of AME-6 in the solid state (Figure 9a). Moreover, the herringbone architecture is also

stabilized by weak intermolecular C–H... π (D_5 ; $E_{\text{tot}} = -2.9$ kcal mol⁻¹) and C–H...Cl (D_6 ; $E_{\text{tot}} = -2.5$ kcal mol⁻¹) interactions (Figure 9b). Overall, the dispersion energies contribute more than 64% toward the stabilization.

In AME-7, there are two crystallographically independent molecules observed in the asymmetric unit. The crystal packing is somewhat similar to those of AME-6 (Figure 8) and AME-3. However, there are differences in the molecular arrangements within the herringbone architectures of AME-7 and AME-3. The PIXEL energy analysis identifies a total of eight molecular pairs (D_1 – D_8 ; $-17.9 < E_{\text{tot}} > -1.0$ kcal mol⁻¹; Figure S14) from the crystal structure of AME-7. Among the eight dimers, two of the dimers are generated by the self-association of molecule A and its symmetry-related partners (D_{2AA} and D_{3AA}). Three dimers are produced by molecule B and its symmetry-related partners (D_{1BB} , D_{4BB} , and D_{8BB}). Similarly, three dimers are constructed from A/B or B/A pair of molecules (D_{5AB} – D_{7AB}). The dimers generated by molecules of A and molecules of B are different. The strong dimer D_{1BB} is formed by molecular stacking of symmetry-related molecules of B. This dimer is also supported by the C–H... π interaction. Within the molecular stacking, the centroid to centroid distance between resonance-assisted pseudorings is 4.067 Å. In contrast, dimer D_{2AA} is formed with similar strength in comparison to D_{1BB} by molecular stacking in which the centroid to centroid distance between resonance-assisted pseudorings is 3.876 Å. Dimer D_{3AA} is generated by molecular stacking in which the separation between centroids of the resonance-assisted rings is 3.590 Å. The strength of dimer D_{3AA} is comparable to that of D_{4BB} , and the latter dimer is stabilized by an intermolecular C–H...O interaction in which the ester C=O group is involved as an acceptor. This interaction generates a closed loop that has a graph set motif of $R_2^2(18)$. These neighboring closed loops are connected by a homohalogen contact (Cl3...Cl4; D_{8BB} ; Figure 10a) in which the shortest distance between two chlorine atoms is 3.492(1) Å. As was noted earlier, molecules A and B generate three dimers and these dimers are stabilized by intermolecular C–H...O, C–H... π , N–H...Cl, C–H...Cl, and Cl...O=C

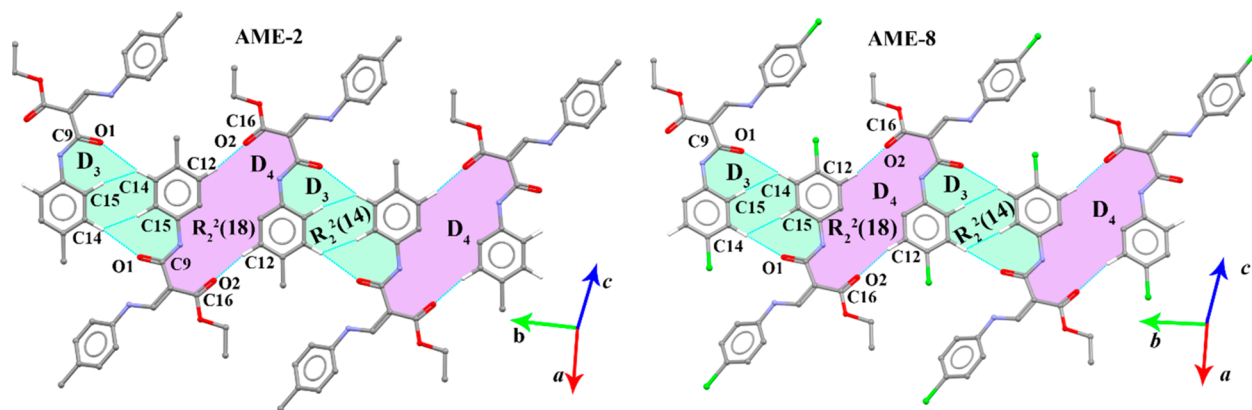


Figure 11. C–H...O interactions in D_3 and D_4 linking the neighboring molecules into a molecular sheet in AME-2 and AME-8 which forms parallel to the b axis.

interactions. The strong dimer D_{5AB} is formed between molecules A and B via N–H...Cl, Cl...O=C, and C–H...C interactions. The adjacent dimers of D_{5AB} are interlinked by an intermolecular C18–H18B...Cg2B interaction in dimer D_{6AB} and the Cl3...Cl4 contact in D_{8BB} (Figure 10b). The D_{7AB} dimer is stabilized by an intermolecular C–H...Cl (involving H17A and Cl3) interaction.

The structure of AME-8, a 4-Cl derivative, is isotopic with its 4-Me counterpart (AME-2). Although the crystal structure of ethyl (*E*)-3-(4-methylanilino)-2-[(4-methylphenyl)carbamoyl]prop-2-enoate (4-Me derivative) has been reported by Islor et al.,⁷² we used our redetermined structure of AME-2 for all analyses used in this study. In both cases, there are six dimers identified by the PIXEL energy analysis and all of the dimers are identical in both structures except for the least stable dimer D_6 (Figures S9 and S15). The molecules are packed as double-helical-like chains, and each chain runs in the opposite direction with respect to the orientation of another chain in a double-helical-like arrangement (Figure 8). The crystal packing of these molecules is similar to that of AME-5 (4-OMe). All of the *para*-substituted (4-Cl, 4-Me, and 4-OMe) amido esters show similar packing features. In AME-8 and AME-2, the strong dimer D_1 is generated by the molecular stacking in which resonance-assisted rings are stacking. The molecular stacking is closer in AME-2 in comparison to AME-8, as is evident from the centroid to centroid distance of molecular pairs (see Table 3).

The dimer D_1 is also supported by an intermolecular C–H...O interaction, in which the ester carbonyl group acts as an acceptor. Dimer D_2 is stabilized by three-centered interactions, one of which is a C–H...O interaction and the remaining one is a C–H...Cg(π) interaction (Cg is the centroid of the resonance-assisted ring). Dimers D_3 and D_4 are formed by intermolecular C–H...O interactions in which both C=O groups are involved as acceptors and generate alternate closed-loop motifs (Figure 11). The former dimer has an $R_2^2(14)$ ring motif, while the latter dimer has an $R_2^2(18)$ ring motif. Dimer D_5 is stabilize by an intermolecular C–H... π interaction in which the centroid of ring II is involved as an acceptor. As was mentioned earlier, the only difference observed between the isomorphous structures is the formation of the least stable dimer: i.e., D_6 . In AME-8, this dimer is stabilized by a Cl11... π (Cg2) interaction, whereas in AME-2 the corresponding dimer is stabilized by an intermolecular C–H... π (Cg2) interaction.

Moreover, the intermolecular interaction is slightly stronger for the latter dimer in comparison to the former dimer.

Isostructurality Analysis. A structural similarity analysis was performed for all possible pairs of structures with the XPac 2.0 program developed by Gelbrich and coauthors.^{73–75} This method provides information on the degree of packing similarity: i.e., the dissimilarity index (x) and the stretching parameter (Table 4).

Table 4. Structural Similarity Parameters for AME-1–8

| combination | dissimilarity index (x) | stretching parameter (Å) | Δa (deg) | Δp (deg) |
|---------------|-----------------------------|--------------------------|------------------|------------------|
| 3D Similarity | | | | |
| AME-2 AME-8 | 1.6 | 0.16 | 0.5 | 1.5 |
| 2D Similarity | | | | |
| AME-5 AME-8 | 13.4 | 0.56 | 7.6 | 11.0 |
| 1D Similarity | | | | |
| AME-2 AME-5 | 11.1 | 0.50 | 5.9 | 9.4 |
| 0D Similarity | | | | |
| AME-1 AME-2 | 11.7 | 0.18 | 5.6 | 10.3 |
| AME-1 AME-5 | 7.5 | 0.21 | 4.4 | 6.1 |
| AME-1 AME-6 | 5.2 | 0.04 | 2.5 | 4.5 |
| AME-1 AME-7 | 6.1 | 0.21 | 4.1 | 4.5 |
| AME-1 AME-8 | 12.1 | 0.22 | 6.0 | 10.5 |
| AME-2 AME-4 | 13.9 | 0.89 | 7.6 | 11.6 |
| AME-2 AME-7 | 4.6 | 0.17 | 2.6 | 3.9 |
| AME-3 AME-4 | 11.3 | 0.33 | 1.8 | 11.2 |
| AME-3 AME-7 | 10.1 | 0.12 | 6.0 | 8.2 |
| AME-5 AME-6 | 7.5 | 0.17 | 3.8 | 6.5 |
| AME-5 AME-7 | 11.7 | 0.01 | 7.6 | 8.9 |
| AME-6 AME-7 | 7.2 | 0.18 | 4.8 | 5.3 |
| AME-7 AME-8 | 5.6 | 0.13 | 3.2 | 4.6 |

For each pair of structures, the XPac program identifies one of the following structural similarities: i.e., 0D (discrete assembly match or a dimer match), 1D (row of molecules match), 2D (layer of molecules match), and 3D (isostructural). From the analysis, we found that most of the combinations show an 0D structural similarity: i.e., a dimer match. The AME-1 structure shares 0D structural similarity with 4-Me (AME-2), 4-OMe (AME-5), 2-Cl (AME-6), 3-Cl (AME-7), and 4-Cl (AME-8, Figure 12) This dimer is primarily stabilized by the stacking of resonance-assisted rings. The intermolecular interactions energies for this dimer in different structures are comparable. The 4-Me and 3-OMe

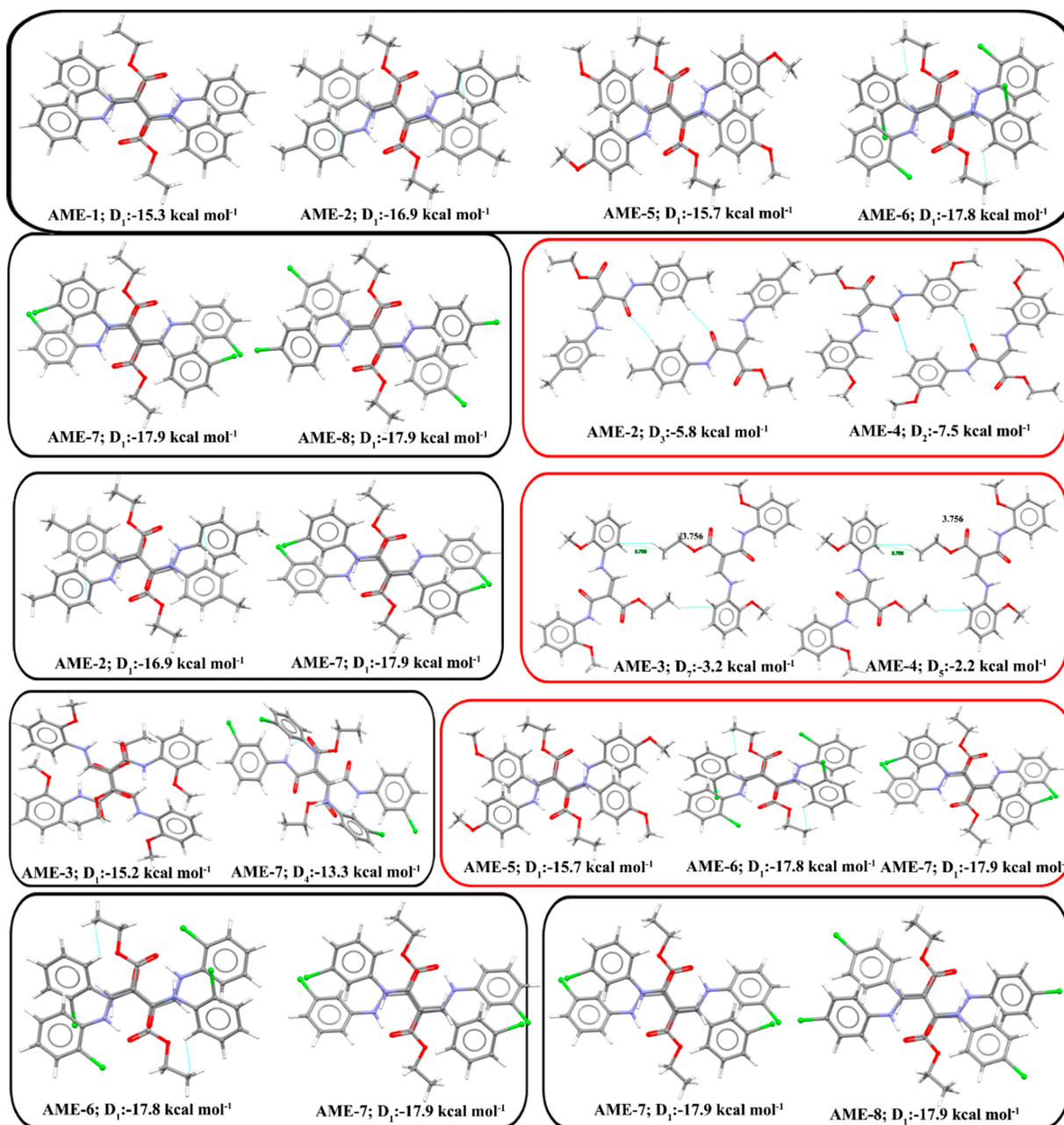


Figure 12. Structural OD similarities of AME-1–8.

structures show OD structural similarity. This dimer (D_2) is stabilized by an intermolecular C–H \cdots O interaction (involving amide C=O as an acceptor). This dimer is slightly more stable in 3-OMe than in 4-Me. Similarly, AME-3 and AME-4 also share OD structural similarity. In this case, the methyl group of the ester moiety in each molecule of the dimer is in close proximity (Figure S14). It is important to note that AME-2 and AME-5 share 1D structural similarity in which the adjacent dimer D_1 is arranged in an offset mode (Figure S16). A 2D structural similarity is observed for AME-5 and AME-8. In both structures, the basic motif formed by the molecular stacking runs in both directions (Figure S17). Since AME-2 and AME-8 are isomorphous, they show 3D structural similarity. Overall, this analysis helps to identify the common motifs occurring in these derivatives and suggests that the motif formed by molecular stacking involving resonance-assisted rings is the most preferred choice.

Topological Analysis of Intermolecular C–H \cdots O and C–H \cdots C (π) Interactions. To evaluate the strength of various intermolecular interactions in the selected molecular dimers in AME-1–AME-8, the topological parameters at their bond critical points (BCPs) were calculated. The topological parameters for intermolecular interactions and the molecular graphs of dimers are presented in Tables S6–S13 and Figures S18–S25 in the Supporting Information. In all eight structures, the observed intermolecular interactions are closed-shell in nature as evaluated using the following conditions: (i) $\nabla^2\rho > 0$, (ii) $| -V/G | < 1$, and (iii) $H > 0$. Moreover, the electron density values for all C–H \cdots O interactions observed in these structures satisfy the Koch and Popelier limit ($0.013 \text{ e } \text{\AA}^{-3} < \rho < 0.236 \text{ e } \text{\AA}^{-3}$) suggested for hydrogen bonds.⁷⁶ The dissociation energies for the C–H \cdots O interactions in these structures are in the range of 0.72–1.73 kcal mol⁻¹. All of the C–H \cdots C interactions observed in these structures are closed-

shell bonding in nature. Further, the electron density values for the C–H⋯C interactions in AME-1–8 are in the range of $0.027 \text{ e } \text{Å}^{-3} < \rho > 0.052 \text{ e } \text{Å}^{-3}$ and are found to be within the Koch and Popelier limit for hydrogen bonds and are comparable to those in an earlier experimental charge density analysis.⁷⁷ As expected, the dissociation energies for these interactions are in the range $0.55\text{--}1.14 \text{ kcal mol}^{-1}$.

Energy Frameworks and Lattice Energy. The total lattice energies were calculated for AME-1–8 using the PIXEL method, and these energies along with the different energy components are summarized in Table 5.

Table 5. Lattice Energies (kcal mol^{-1}) Partitioned into Coulombic, Polarization, Dispersion, and Repulsion Contributions for AME-1–8

| compound | E_{Coul} | E_{pol} | E_{disp} (% E_{disp}) | E_{rep} | E_{tot} |
|----------|-------------------|------------------|--|------------------|------------------|
| AME-1 | −7.96 | −3.63 | −38.98 (77) | 19.05 | −31.52 |
| AME-2 | −12.07 | −5.31 | −49.43 (74) | 30.69 | −36.11 |
| AME-3 | −11.78 | −4.78 | −43.19 (72) | 22.92 | −36.85 |
| AME-4 | −10.66 | −4.78 | −46.22(75) | 24.98 | −36.71 |
| AME-5 | −12.69 | −4.92 | −49.16(74) | 27.77 | −39.01 |
| AME-6 | −9.53 | −4.13 | −45.46 (77) | 23.11 | −36.04 |
| AME-7 | −10.18 | −4.28 | −47.44 (77) | 24.28 | −37.62 |
| AME-8 | −11.23 | −4.49 | −49.62 (76) | 26.46 | −38.89 |

The results suggest that the unsubstituted, parent compound AME-1 is weakly packed ($E_{\text{tot}} = -31.5 \text{ kcal mol}^{-1}$) in the solid state in comparison to the other crystal structures (AME-2–8; $-36.0 < E_{\text{tot}} > -39.0 \text{ kcal mol}^{-1}$). Among the methoxy isomers (AME-3–5), the crystal structure of the 4-methoxy derivative is found to be the most stable (AME-5, $E_{\text{tot}} = -39.0 \text{ kcal mol}^{-1}$). However, the lattice energies for the 2-OMe (AME-3, $E_{\text{tot}} = -36.9 \text{ kcal mol}^{-1}$) and 3-OMe derivatives (AME-4, $E_{\text{tot}} = -36.7 \text{ kcal mol}^{-1}$) are comparable. Similarly, the structure of the 4-Cl (AME-8) derivative is found to be more than stable than other two Cl isomers. The stability of the Cl isomers is in

the order $4\text{-Cl} > 3\text{-Cl} > 2\text{-Cl}$. Moreover, the stabilities of the 4-OMe and 4-Cl derivatives are comparable. However, the stability is reduced by $\sim 3 \text{ kcal mol}^{-1}$ due to 4-Me substitution. In all of the structures, the dispersion energy contributes more than 72% toward the stabilization.

To rationalize the mechanical behavior of crystals used in the present study at the molecular level, we determined energy frameworks using the CrystalExplorer-17.5 program.⁶⁰ Two different cylinders (green, dispersion energy; blue, total energy; Figure 13) with varying magnitudes are depicted in the energy frameworks diagrams. In AME-1, the zigzag large green cylinders correspond to dimers D_1 and D_2 formed by molecular stacking and these dimers are arranged alternately and run parallel to the a axis. The adjacent zigzag chains are interlinked by small cylinders which represent dimer D_4 formed by a weak intermolecular C–H⋯O interaction. The 3-OMe and 4-OMe derivatives (AME-4 and AME-5) show similar 3D topologies of the energy frameworks in comparison to AME-1. In AME-4, dimer D_1 generates the zigzag chain, whereas two dimers (D_1 and D_2) are arranged in an alternate fashion which produces zigzag chains in AME-5. The small cylinders interconnect the neighboring zigzag chains. The intermolecular C–H⋯C and C–H⋯O interactions formed in molecules of AME-4 and AME-5 are shown as small cylinders.

The topology of the energy framework for 2-Cl the derivative is very similar to those of AME-1, AME-4, and AME-5. The vertical zigzag chain is comprised of alternate dimers D_1 and D_2 . The adjacent zigzag chains are interconnected by small cylinders. In this case, intermolecular C–H⋯O and C–H⋯Cl interactions constitute the small cylinders. The 3D energy topology for AME-3 is somewhat similar to that of other structures with respect to the zigzag chain, which is primarily generated by the first two strong dimers (D_1 and D_2). Overall, this analysis suggests that the crystals of AME-1,2,4–8 could have similar mechanical properties irrespective of the different substituents. It also suggests that the stacking of the resonance-assisted rings plays

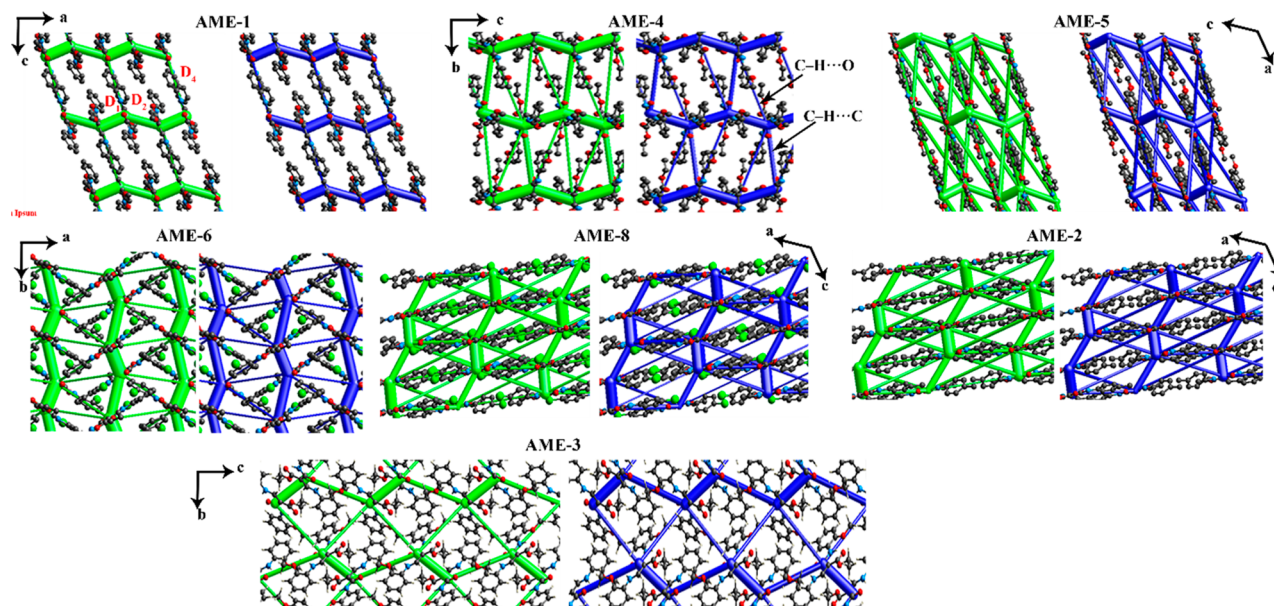


Figure 13. Energy frameworks for the crystal structures of AME-1–8, except for AME-7. Color scheme: blue, total energy; green, dispersion energy. All diagrams use the same cylinder scale of 80 kJ mol^{-1} for energies, and energies with a magnitude of less than 10 kJ mol^{-1} for all for the structures except for AME-3 (a $<20 \text{ kJ mol}^{-1}$ cutoff was used) have been omitted for clarity.

an important role in providing the similar mechanical properties. It is interesting to note that AME-7 shows a completely different 3D topology of the energy framework in comparison to the other structures. It shows a ladderlike topology instead of zigzag chains. This feature suggests that the crystals of AME-7 could have completely different mechanical properties in comparison to the other crystals.

CONCLUSIONS

In the present study, we have systematically explored the effect of substituents on the crystal packing and intramolecular RAHB and non-RAHB and weak intermolecular interactions in AME-1–8. In all structures reported herein, an angularly fused pseudotricyclic (*S*(6),*S*(6),*S*(6)) ring system has been formed by the intramolecular N–H···O and C–H···O interactions. The weak intermolecular interactions in AME-1–8 were quantitatively analyzed by PIXEL, DFT, and QTAIM approaches. The PIXEL energy calculations revealed that the strong dimer D_1 was formed by the molecular stacking involving pseudorings of RAHBs. Most of the structures shared a 0D structural similarity, and AME-2 and AME-5 showed a 1D structural similarity. AME-5 and AME-8 displayed a 2D structural similarity. The 3D topologies of the energy frameworks show similar features, suggesting that they may have similar mechanical properties. All of the weak intermolecular C–H···O, C–H··· π , and C–H···Cl interactions are closed-shell in nature, as evaluated by the topological parameters derived with the QTAIM framework. The topological analysis for X-ray and optimized structures in the gas phase suggested differences in the natures and strengths of intramolecular RAHBs and non-RAHBs. We found that the strengths and the nature of these intramolecular N–H···O hydrogen bonding were modulated by the crystal packing effect. A pronounced effect was observed for a RAHB in comparison to a non-RAHB. The variations in the bond path values indicated the effect of electron-donating and -withdrawing groups introduced in the amido ester. Moreover, the amide group acidity is more pronounced in electron-withdrawing structures than in the electron-donating derivatives.

ASSOCIATED CONTENT

Supporting Information

The Supporting Information is available free of charge at <https://pubs.acs.org/doi/10.1021/acs.cgd.0c01010>.

Synthesis procedures along with the spectral data for AME-1–8, selected torsion angles, selected topological parameters for intramolecular interactions in the optimized molecules and molecular graphs, discussion of the Hirshfeld surface analysis and 2D fingerprint plots, molecular electrostatic surface potentials (MESPs), intermolecular interactions, structures of selected molecular dimers in each compound along with the interaction energies, and selected topological parameters for various intermolecular interactions and their molecular graphs (PDF)

Accession Codes

CCDC 655619, 664991, 665885–665886, 678846, 804832–804833, and 804925 contain the supplementary crystallographic data for this paper. These data can be obtained free of charge via www.ccdc.cam.ac.uk/data_request/cif, or by emailing data_request@ccdc.cam.ac.uk, or by contacting The

Cambridge Crystallographic Data Centre, 12 Union Road, Cambridge CB2 1EZ, UK; fax: +44 1223 336033.

AUTHOR INFORMATION

Corresponding Authors

Subbiah Thamocharan – Biomolecular Crystallography Laboratory, Department of Bioinformatics, School of Chemical and Biotechnology, SASTRA Deemed University, Thanjavur 613 401, India; orcid.org/0000-0003-2758-6649; Email: thamu@scbt.sastra.edu

Andivelu Ilangoan – School of Chemistry, Bharathidasan University, Tiruchirappalli 620 024, Tamilnadu, India; orcid.org/0000-0001-7240-7166; Email: ilangoan@bdu.ac.in

Authors

Perumal Venkatesan – School of Chemistry, Bharathidasan University, Tiruchirappalli 620 024, Tamilnadu, India; Unidad de Polímeros y Electrónica Orgánica, Instituto de Ciencias, Benemérita Universidad Autónoma de Puebla, San Pedro Zacachimalpa, Puebla, México; orcid.org/0000-0001-6134-8324

M. Judith Percino – Unidad de Polímeros y Electrónica Orgánica, Instituto de Ciencias, Benemérita Universidad Autónoma de Puebla, San Pedro Zacachimalpa, Puebla, México; orcid.org/0000-0003-1610-7155

Complete contact information is available at: <https://pubs.acs.org/10.1021/acs.cgd.0c01010>

Notes

The authors declare no competing financial interest.

ACKNOWLEDGMENTS

The authors thank the DST-India (FIST program) for the use of the Bruker SMART APEX II diffractometer and the 400 MHz NMR facility at the School of Chemistry, Bharathidasan University. The authors thank the Laboratorio Nacional de Supercomputo del Sureste (LNS-BUAP) for the calculation service and the VIEP-BUAP (project 100184100-VIEP).

REFERENCES

- (1) Karas, L. J.; Wu, C.-H.; Das, R.; Wu, J. I. C. Hydrogen bond design principles. *Wiley Interdiscip. Rev.: Comput. Mol. Sci.* **2020**, *10*, e1477 and references cited therein.
- (2) Gilli, G.; Gilli, P. Towards a unified hydrogen-bond theory. *J. Mol. Struct.* **2000**, *552*, 1–15.
- (3) Jesus, A. J. L.; Redinha, J. S. Charge-Assisted Intramolecular Hydrogen Bonds in Disubstituted Cyclohexane Derivatives. *J. Phys. Chem. A* **2011**, *115*, 14069–14077.
- (4) Aakeröy, C. B.; Beatty, A. M.; Lorimer, K. R. Charge-Assisted Hydrogen Bonds and Halogen-Halogen Interactions in Organic Salts: Benzylammonium Benzoates and Pentafluorobenzoates. *Struct. Chem.* **1999**, *10*, 229–242.
- (5) Cleland, W. W.; Kreevoy, M. M. Low-barrier hydrogen bonds and enzymic catalysis. *Science* **1994**, *264*, 1887.
- (6) Gilli, P.; Bertolasi, V.; Pretto, L.; Lyčka, A.; Gilli, G. The Nature of Solid-State N–H···O/O–H···N Tautomeric Competition in Resonant Systems. Intramolecular Proton Transfer in Low-Barrier Hydrogen Bonds Formed by the $\cdots\text{OC}-\text{CN}-\text{NH}\cdots \rightleftharpoons \cdots\text{HO}-\text{CC}-\text{NN}\cdots$ Ketohydrazone–Azoenol System. A Variable-Temperature X-ray Crystallographic and DFT Computational Study. *J. Am. Chem. Soc.* **2002**, *124*, 13554–13567.
- (7) Lough, A. J.; Park, S.; Ramachandran, R.; Morris, R. H. Switching On and Off a New Intramolecular Hydrogen-Hydrogen Interaction and the Heterolytic Splitting of Dihydrogen. *Crystal and*

Molecular Structure of $[\text{Ir}\{\text{H}(\eta^1\text{-SC}_3\text{H}_4\text{NH})\}_2(\text{PCy}_3)_2]\text{BF}_4 \cdot 2.7\text{CH}_2\text{Cl}_2$. *J. Am. Chem. Soc.* **1994**, *116*, 8356–8357.

(8) Lee, J. C.; Peris, E.; Rheingold, A. L.; Crabtree, R. H. An Unusual Type of H...H Interaction: Ir-H...H-O and Ir-H...H-N Hydrogen Bonding and Its Involvement in σ -Bond Metathesis. *J. Am. Chem. Soc.* **1994**, *116*, 11014–11019.

(9) Gilli, G.; Bellucci, F.; Ferretti, V.; Bertolasi, V. Evidence for resonance-assisted hydrogen bonding from crystal-structure correlations on the enol form of the β -diketone fragment. *J. Am. Chem. Soc.* **1989**, *111*, 1023–1028.

(10) Bertolasi, V.; Gilli, P.; Ferretti, V.; Gilli, G. Evidence for resonance-assisted hydrogen bonding. 2. Interrelation between crystal structure and spectroscopic parameters in eight intramolecularly hydrogen bonded 1,3-diaryl-1,3-propanedione enols. *J. Am. Chem. Soc.* **1991**, *113*, 4917–4925.

(11) Jiang, X.; Zhang, H.; Wu, W.; Mo, Y. A Critical Check for the Role of Resonance in Intramolecular Hydrogen Bonding. *Chem. - Eur. J.* **2017**, *23*, 16885–16891.

(12) Gilli, P.; Bertolasi, V.; Ferretti, V.; Gilli, G. Evidence for resonance-assisted hydrogen bonding. 4. Covalent nature of the strong homonuclear hydrogen bond. Study of the O-H...O system by crystal structure correlation methods. *J. Am. Chem. Soc.* **1994**, *116*, 909–915.

(13) Gilli, P.; Bertolasi, V.; Pretto, L.; Antonov, L.; Gilli, G. Variable-Temperature X-ray Crystallographic and DFT Computational Study of the NH...O/N...HO Tautomeric Competition in 1-(Aryloxy)-2-naphthols. Outline of a Transition-State Hydrogen-Bond Theory. *J. Am. Chem. Soc.* **2005**, *127*, 4943–4953.

(14) Gilli, P.; Bertolasi, V.; Pretto, L.; Ferretti, V.; Gilli, G. Covalent versus Electrostatic Nature of the Strong Hydrogen Bond: Discrimination among Single, Double, and Asymmetric Single-Well Hydrogen Bonds by Variable-Temperature X-ray Crystallographic Methods in β -Diketone Enol RAHB Systems. *J. Am. Chem. Soc.* **2004**, *126*, 3845–3855.

(15) Chin, J.; Kim, D. C.; Kim, H.-J.; Panosyan, F. B.; Kim, K. M. Chiral Shift Reagent for Amino Acids Based on Resonance-Assisted Hydrogen Bonding. *Org. Lett.* **2004**, *6*, 2591–2593.

(16) Park, H.; Kim, K. M.; Lee, A.; Ham, S.; Nam, W.; Chin, J. Bioinspired Chemical Inversion of L-Amino Acids to D-Amino Acids. *J. Am. Chem. Soc.* **2007**, *129*, 1518–1519.

(17) Mahmudov, K. T.; Pombeiro, A. J. L. Resonance-Assisted Hydrogen Bonding as a Driving Force in Synthesis and a Synthone in the Design of Materials. *Chem. - Eur. J.* **2016**, *22*, 16356–16398.

(18) Goswami, S.; Manna, A.; Paul, S.; Das, A. K.; Aich, K.; Nandi, P. K. Resonance-assisted hydrogen bonding induced nucleophilic addition to hamper ESPT: ratiometric detection of cyanide in aqueous media. *Chem. Commun.* **2013**, *49*, 2912–2914.

(19) Li, Q.; Zhang, J.-h.; Cai, Y.; Qu, W.-j.; Gao, G.-y.; Lin, Q.; Yao, H.; Zhang, Y.-m.; Wei, T.-b. A facile colorimetric and fluorescent cyanide chemosensor: utilization of the nucleophilic addition induced by resonance-assisted hydrogen bond. *Tetrahedron* **2015**, *71*, 857–862.

(20) Saccone, M.; Pfletscher, M.; Kather, S.; Wölper, C.; Daniliuc, C.; Mezger, M.; Giese, M. Improving the mesomorphic behaviour of supramolecular liquid crystals by resonance-assisted hydrogen bonding. *J. Mater. Chem. C* **2019**, *7*, 8643–8648.

(21) Chin, J.; Mancin, F.; Thavarajah, N.; Lee, D.; Lough, A.; Chung, D. S. Controlling Diaza-Cope Rearrangement Reactions with Resonance-Assisted Hydrogen Bonds. *J. Am. Chem. Soc.* **2003**, *125*, 15276–15277.

(22) Kim, H.; Nguyen, Y.; Yen, C. P.-H.; Chagal, L.; Lough, A. J.; Kim, B. M.; Chin, J. Stereospecific Synthesis of C2 Symmetric Diamines from the Mother Diamine by Resonance-Assisted Hydrogen-Bond Directed Diaza-Cope Rearrangement. *J. Am. Chem. Soc.* **2008**, *130*, 12184–12191.

(23) Lee, D.-N.; Kim, H.; Mui, L.; Myung, S.-W.; Chin, J.; Kim, H.-J. Electronic Effect on the Kinetics of the Diaza-Cope Rearrangement. *J. Org. Chem.* **2009**, *74*, 3330–3334.

(24) Marković, R.; Shirazi, A.; Džambaski, Z.; Baranac, M.; Minić, D. Configurational isomerization of push–pull thiazolidinone derivatives controlled by intermolecular and intramolecular RAHB: ^1H NMR dynamic investigation of concentration and temperature effects. *J. Phys. Org. Chem.* **2004**, *17*, 118–123.

(25) Bertolasi, V.; Ferretti, V.; Gilli, P.; Gilli, G.; Issa, Y. M.; Sherif, O. E. Intramolecular N-H...O hydrogen bonding assisted by resonance. Part 2. Interrelation between structural and spectroscopic parameters for five 1,3-diketone arylhydrazones derived from dibenzoylmethane. *J. Chem. Soc., Perkin Trans. 2* **1993**, *11*, 2223–2228.

(26) Gilli, P.; Bertolasi, V.; Ferretti, V.; Gilli, G. Evidence for Intramolecular N-H...O Resonance-Assisted Hydrogen Bonding in β -Enaminones and Related Heterodienes. A Combined Crystal-Structural, IR and NMR Spectroscopic, and Quantum-Mechanical Investigation. *J. Am. Chem. Soc.* **2000**, *122*, 10405–10417.

(27) Bertolasi, V.; Gilli, P.; Ferretti, V.; Gilli, G.; Fernandez-Castano, C. Self-assembly of NH-pyrazoles via intermolecular N-H...N hydrogen bonds. *Acta Crystallogr., Sect. B: Struct. Sci.* **1999**, *55*, 985–993.

(28) Bertolasi, V.; Gilli, P.; Ferretti, V.; Gilli, G. Intermolecular N-H...O Hydrogen Bonding Assisted by Resonance. II. Self Assembly of Hydrogen-Bonded Secondary Enaminones in Supramolecular Catemers. *Acta Crystallogr., Sect. B: Struct. Sci.* **1998**, *54*, 50–65.

(29) Palusiak, M.; Simon, S.; Solà, M. Interplay between Intramolecular Resonance-Assisted Hydrogen Bonding and Aromaticity in *o*-Hydroxyaryl Aldehydes. *J. Org. Chem.* **2006**, *71*, 5241–5248.

(30) Rybarczyk-Pirek, A. J.; Grabowski, S. J.; Malecka, M.; Nawrot-Modranka, J. Crystal and Molecular Structures of New Chromone Derivatives as Empirical Evidence of Intramolecular Proton Transfer Reaction; Ab Initio Studies on Intramolecular H-Bonds in Enaminones. *J. Phys. Chem. A* **2002**, *106*, 11956–11962.

(31) Wojtulewski, S.; Grabowski, S. J. Different donors and acceptors for intramolecular hydrogen bonds. *Chem. Phys. Lett.* **2003**, *378*, 388–394.

(32) Sanz, P.; Yáñez, M.; Mó, O. Competition between X...H...Y Intramolecular Hydrogen Bonds and X...Y (X = O, S, and Y = Se, Te) Chalcogen–Chalcogen Interactions. *J. Phys. Chem. A* **2002**, *106*, 4661–4668.

(33) Beck, J. F.; Mo, Y. How resonance assists hydrogen bonding interactions: An energy decomposition analysis. *J. Comput. Chem.* **2007**, *28*, 455–466.

(34) Nassour, A.; Kubicki, M.; Wright, J.; Borowiak, T.; Dutkiewicz, G.; Lecomte, C.; Jelsch, C. Charge-density analysis using multipolar atom and spherical charge models: 2-methyl-1,3-cyclopentanedione, a compound displaying a resonance-assisted hydrogen bond. *Acta Crystallogr., Sect. B: Struct. Sci., Cryst. Eng. Mater.* **2014**, *70*, 197–211.

(35) Pareras, G.; Palusiak, M.; Duran, M.; Solà, M.; Simon, S. Tuning the Strength of the Resonance-Assisted Hydrogen Bond in *o*-Hydroxybenzaldehyde by Substitution in the Aromatic Ring I. *J. Phys. Chem. A* **2018**, *122*, 2279–2287.

(36) Bertolasi, V.; Gilli, P.; Ferretti, V.; Gilli, G.; Vaughan, K. Interplay between steric and electronic factors in determining the strength of intramolecular resonance-assisted NH...O hydrogen bond in a series of β -ketoarylhidrazones. *New J. Chem.* **1999**, *23*, 1261–1267.

(37) Bertolasi, V.; Pretto, L.; Ferretti, V.; Gilli, P.; Gilli, G. Interplay between steric and electronic factors in determining the strength of intramolecular N-H...O resonance-assisted hydrogen bonds in β -enaminones. *Acta Crystallogr., Sect. B: Struct. Sci.* **2006**, *62*, 1112–1120.

(38) Palusiak, M.; Simon, S.; Solà, M. Interplay between Intramolecular Resonance-Assisted Hydrogen Bonding and Local Aromaticity. II. 1,3-Dihydroxyaryl-2-aldehydes. *J. Org. Chem.* **2009**, *74*, 2059–2066.

(39) Fonseca Guerra, C.; Bickelhaupt, F. M.; Snijders, J. G.; Baerends, E. J. The Nature of the Hydrogen Bond in DNA Base Pairs:

The Role of Charge Transfer and Resonance Assistance. *Chem. - Eur. J.* **1999**, *5*, 3581–3594.

(40) Guillaumes, L.; Simon, S.; Fonseca Guerra, C. The Role of Aromaticity, Hybridization, Electrostatics, and Covalency in Resonance-Assisted Hydrogen Bonds of Adenine–Thymine (AT) Base Pairs and Their Mimics. *ChemistryOpen* **2015**, *4*, 318–327.

(41) Cole, J. M.; Lin, T.-C.; Ashcroft, C. M.; Perez-Moreno, J.; Tan, Y.; Venkatesan, P.; Higginbotham, A. P.; Pattison, P.; Edwards, A. J.; Piltz, R. O.; Clays, K.; Ilangovan, A. Relating the Structure of Geminal Amido Esters to their Molecular Hyperpolarizability. *J. Phys. Chem. C* **2016**, *120*, 29439–29448.

(42) Bader, R. F. W. *Atoms in Molecules: A Quantum Theory*; Clarendon Press: 1994.

(43) Bader, R. F. W. A Quantum-Theory of Molecular-Structure and Its Applications. *Chem. Rev.* **1991**, *91*, 893–928.

(44) Spackman, M. A.; Jayatilaka, D. Hirshfeld surface analysis. *CrystEngComm* **2009**, *11*, 19–32.

(45) McKinnon, J. J.; Spackman, M. A.; Mitchell, A. S. Novel tools for visualizing and exploring intermolecular interactions in molecular crystals. *Acta Crystallogr., Sect. B: Struct. Sci.* **2004**, *60*, 627–668.

(46) Wood, P. A.; McKinnon, J. J.; Parsons, S.; Pidcock, E.; Spackman, M. A. Analysis of the compression of molecular crystal structures using Hirshfeld surfaces. *CrystEngComm* **2008**, *10*, 368–376.

(47) Spackman, M. A.; McKinnon, J. J. Fingerprinting intermolecular interactions in molecular crystals. *CrystEngComm* **2002**, *4*, 378–392.

(48) Parkin, A.; Barr, G.; Dong, W.; Gilmore, C. J.; Jayatilaka, D.; McKinnon, J. J.; Spackman, M. A.; Wilson, C. C. Comparing entire crystal structures: structural genetic fingerprinting. *CrystEngComm* **2007**, *9*, 648–652.

(49) Ilangovan, A.; Kumar, R. G., 2,2-Bis(ethoxycarbonyl)vinyl (BECV) as a Versatile Amine Protecting Group for Selective Functional-Group Transformations. *Chem. - Eur. J.* **2010**, *16*, 2938–2943.

(50) Sheldrick, G. Crystal structure refinement with SHELXL. *Acta Crystallogr., Sect. C: Struct. Chem.* **2015**, *71*, 3–8.

(51) Spek, A. Structure validation in chemical crystallography. *Acta Crystallogr., Sect. D: Biol. Crystallogr.* **2009**, *65*, 148–155.

(52) Macrae, C. F.; Edgington, P. R.; McCabe, P.; Pidcock, E.; Shields, G. P.; Taylor, R.; Towler, M.; van de Streek, J. Mercury: visualization and analysis of crystal structures. *J. Appl. Crystallogr.* **2006**, *39*, 453–457.

(53) Macrae, C. F.; Sovago, I.; Cottrell, S. J.; Galek, P. T. A.; McCabe, P.; Pidcock, E.; Platings, M.; Shields, G. P.; Stevens, J. S.; Towler, M.; Wood, P. A. Mercury 4.0: from visualization to analysis, design and prediction. *J. Appl. Crystallogr.* **2020**, *53*, 226–235.

(54) Frisch, M. J.; Trucks, G. W.; Schlegel, H. B.; Scuseria, G. E.; Robb, M. A.; Cheeseman, J. R.; Scalmani, G.; Barone, V.; Mennucci, B.; Petersson, G. A.; Nakatsuji, H.; Caricato, M.; Li, X.; Hratchian, H. P.; Izmaylov, A. F.; Bloino, J.; Zheng, G.; Sonnenberg, J. L.; Hada, M.; Ehara, M.; Toyota, K.; Fukuda, R.; Hasegawa, J.; Ishida, M.; Nakajima, T.; Honda, Y.; Kitao, O.; Nakai, H.; Vreven, T.; Montgomery, J. A.; Peralta, J. E.; Ogliaro, F.; Bearpark, M.; Heyd, J. J.; Brothers, E.; Kudin, K. N.; Staroverov, V. N.; Kobayashi, R.; Normand, J.; Raghavachari, K.; Rendell, A.; Burant, J. C.; Iyengar, S. S.; Tomasi, J.; Cossi, M.; Rega, N.; Millam, J. M.; Klene, M.; Knox, J. E.; Cross, J. B.; Bakken, V.; Adamo, C.; Jaramillo, J.; Gomperts, R.; Stratmann, R. E.; Yazyev, O.; Austin, A. J.; Cammi, R.; Pomelli, C.; Ochterski, J. W.; Martin, R. L.; Morokuma, K.; Zakrzewski, V. G.; Voth, G. A.; Salvador, P.; Dannenberg, J. J.; Dapprich, S.; Daniels, A. D.; Farkas, Foresman, J. B.; Ortiz, J. V.; Cioslowski, J.; Fox, D. J. *Gaussian 16, Rev. C.01*; Gaussian Inc.: Wallingford, CT, 2016.

(55) Zhao, Y.; Schultz, N. E.; Truhlar, D. G. Design of density functionals by combining the method of constraint satisfaction with parametrization for thermochemistry, thermochemical kinetics, and noncovalent interactions. *J. Chem. Theory Comput.* **2006**, *2*, 364–382.

(56) Hohenstein, E. G.; Chill, S. T.; Sherrill, C. D. Assessment of the Performance of the M05-2X and M06-2X Exchange-Correlation

Functionals for Noncovalent Interactions in Biomolecules. *J. Chem. Theory Comput.* **2008**, *4*, 1996–2000.

(57) Grimme, S.; Antony, J.; Ehrlich, S.; Krieg, H. A consistent and accurate ab initio parametrization of density functional dispersion correction (DFT-D) for the 94 elements H–Pu. *J. Chem. Phys.* **2010**, *132*, 154104.

(58) Gavezzotti, A. Non-conventional bonding between organic molecules. The ‘halogen bond’ in crystalline systems. *Mol. Phys.* **2008**, *106*, 1473–1485.

(59) Boys, S. F.; Bernardi, F. The calculation of small molecular interactions by the differences of separate total energies. Some procedures with reduced errors. *Mol. Phys.* **1970**, *19*, 553–566.

(60) Turner, M.; McKinnon, J.; Wolff, S.; Grimwood, D.; Spackman, P.; Jayatilaka, D.; Spackman, M. *CrystalExplorer17*; University of Western Australia: 2017.

(61) Todd, A. K. *AIMALL (Ver. 16.05.18)*; TK Gristmill Software: Overland Park, KS, USA, 2017.

(62) Espinosa, E.; Molins, E.; Lecomte, C. Hydrogen bond strengths revealed by topological analyses of experimentally observed electron densities. *Chem. Phys. Lett.* **1998**, *285*, 170–173.

(63) Gatti, C. Chemical bonding in crystals: new directions. *Z. Kristallogr. - Cryst. Mater.* **2005**, *220*, 399–457.

(64) Blagojević, J. P.; Zarić, S. D. Stacking interactions of hydrogen-bridged rings – stronger than the stacking of benzene molecules. *Chem. Commun.* **2015**, *51*, 12989–12991.

(65) Karabiyik, H.; Karabiyik, H.; Ocak Iskeleli, N. Hydrogen-bridged chelate ring-assisted $[\pi]$ -stacking interactions. *Acta Crystallogr., Sect. B: Struct. Sci.* **2012**, *68*, 71–79.

(66) Roberts, R. M. The reaction of diarylformamides with ethyl malonate¹. *J. Org. Chem.* **1949**, *14*, 277–284.

(67) Sobczyk, L.; Grabowski, S. J.; Krygowski, T. M. Interrelation between H-Bond and π -Electron Delocalization. *Chem. Rev.* **2005**, *105*, 3513–3560.

(68) Góra, R. W.; Maj, M.; Grabowski, S. J. Resonance-assisted hydrogen bonds revisited. Resonance stabilization vs. charge delocalization. *Phys. Chem. Chem. Phys.* **2013**, *15*, 2514–2522.

(69) Blagojević, J. P.; Veljković, D. Ž.; Zarić, S. D. Stacking interactions between hydrogen-bridged and aromatic rings: study of crystal structures and quantum chemical calculations. *CrystEngComm* **2017**, *19*, 40–46.

(70) Blagojević Filipović, J. P.; Hall, M. B.; Zarić, S. D. Stacking Interactions of Resonance-Assisted Hydrogen-Bridged Rings. A Systematic Study of Crystal Structures and Quantum-Chemical Calculations. *Cryst. Growth Des.* **2019**, *19*, 5619–5628.

(71) Blagojević Filipović, J. P.; Hall, M. B.; Zarić, S. D. Stacking interactions of resonance-assisted hydrogen-bridged rings and C6-aromatic rings. *Phys. Chem. Chem. Phys.* **2020**, *22*, 13721–13728.

(72) Islor, A. M.; Garudachari, B.; Gerber, T.; Hosten, E.; Betz, R. Ethyl (Z)-3-(4-methylanilino)-2-[(4-methylphenyl)carbamoyl]prop-2-enoate. *Acta Crystallogr., Sect. E: Struct. Rep. Online* **2012**, *68*, o3218.

(73) Gelbrich, T.; Threlfall, T. L.; Hursthouse, M. B. XPac dissimilarity parameters as quantitative descriptors of isostructurality: the case of fourteen 4,5'-substituted benzenesulfonamido-2-pyridines obtained by substituent interchange involving CF3/I/Br/Cl/F/Me/H. *CrystEngComm* **2012**, *14*, 5454–5464.

(74) Gelbrich, T.; Hursthouse, M. B. A versatile procedure for the identification, description and quantification of structural similarity in molecular crystals. *CrystEngComm* **2005**, *7*, 324–336.

(75) Gelbrich, T.; Hursthouse, M. B. Systematic investigation of the relationships between 25 crystal structures containing the carbamazepine molecule or a close analogue: a case study of the XPac method. *CrystEngComm* **2006**, *8*, 448–460.

(76) Koch, U.; Popelier, P. L. A. Characterization of C–H–O Hydrogen Bonds on the Basis of the Charge Density. *J. Phys. Chem.* **1995**, *99*, 9747–9754.

(77) Munshi, P.; Guru Row, T. N. Exploring the Lower Limit in Hydrogen Bonds: Analysis of Weak C–H...O and C–H... π Interactions in Substituted Coumarins from Charge Density Analysis. *J. Phys. Chem. A* **2005**, *109*, 659–672.